Performance evaluation of U-tube borehole heat exchangers employing nanofluids as the heat carrier fluid

Performance evaluation of U-tube borehole heat exchangers employing nanofluids as the heat carrier fluid

Aminhossein Jahanbin[a,b*], Giovanni Semprini [a], Beatrice Pulvirenti [a]

[a] Department of Industrial Engineering, Alma Mater Studiorum - University of Bologna, Viale Risorgimento 2, 40136 Bologna, Italy

[b] CIRI - Centro Interdipartimentale di Ricerca Industriale Edilizia e Costruzioni, Alma Mater Studiorum - University of Bologna, Via del Lazzaretto 15/5, 40131Bologna, Italy

*Corresponding author: aminhossein.jahanbin@unibo.it

Abstract.

The present study aims to investigate comprehensively the performance of various nanofluids in single U-tube borehole heat exchangers (BHEs). Seven common nanoparticles with the volume fraction ranging from 0.1% to 2.0% are selected to be evaluated as heat carrier fluid. Firstly, a comparative techno-economic analysis is performed to highlight the merits and drawbacks of each nanofluid. Then, a sensitivity analysis is performed to optimise the decrement percentage of BHE thermal resistance. Finally, by means of the linear regression of numerical results obtained for different nanofluids, simple equations are proposed allowing evaluation of the outlet fluid temperature for nanofluids. The obtained results indicate that Ag- and Cu-based nanofluids are characterised by the highest heat transfer enhancement, although this improvement is at penalty of a higher pressure drop and up to 31% higher required pumping power. The optimum decrement percentage of thermal resistance yielded in presence of Cu-water nanofluid was equal to 4.31%. Economic analysis revealed that the cost of electrical energy for nanofluids due to the higher energy consumption of pump is negligible in comparison with the capital cost of nanoparticles. The SiO_2 nanoparticles with a capital cost ranging from 5.8 to 17.5 €/m was the cheapest nanoparticle to employ, unlike the Ag nanoparticles.

Keywords: Geothermal energy; ground source heat pumps; borehole heat exchangers; ground heat exchangers; nanofluids

1. Introduction

Geothermal energy is one of the most promising renewable energy sources, employable to shift from a fossil-based development to a sustainable development. The direct utilisation of geothermal energy in conjunction with ground-source heat pumps (GSHPs) has shown a great potential for the heating and cooling of buildings as well as production of the domestic hot water. The annual utilisation of thermal energy produced by GSHPs increased by about 40% from 2010 to 2015, with an annual growth rate of 7% [1]. They are eco-friendly and economically advantageous systems compared to traditional heating/cooling systems [2]. The U.S. Environment Protection Agency (EPA) has introduced the GSHPs as the most energy-efficient and environmentally friendly air-conditioning technology [3]. Therefore, development of GSHP systems can remarkably reduce the primary energy consumption and the emission of greenhouse gases from fossil-based fuels.

Ground-coupled heat pumps (GCHPs) emerge as a promising type of GSHPs for the future developments, due to their possibility of installation even where regional laws do not allow groundwater extraction. A GCHP system consists of the vertical or horizontal ground heat exchanger, heat pump, and distribution system. These systems usually employ buried vertical heat exchangers, also called borehole heat exchangers (BHEs). A BHE is generally composed of a single or double high-density polyethylene (HDPE) tube(s) installed in a drilled hole, which is then filled with backfilling materials. In any GCHP system, the BHE is a critical component that needs to be carefully designed since its performance greatly affects the energy efficiency as well as the total cost of the GSHP system [4]. In general, GCHP systems utilising the vertical BHEs have higher coefficients of performance (COP) and require less ground area due to lower seasonal variations in mean temperature of the ground [5]. The performance of GCHP systems has been widely investigated by both simulation tools and experiments [6-8].

Despite the advantages of GCHPs, the central limitations to employ them are their high drilling costs and set-up expenses [9]. In fact, a significant portion of the capital cost of a GCHP can be attributed to boreholes. A study by Blum et al. [10] reported that the installation cost of a borehole in Germany is 40-50 €/m of the BHE depth, while the drilling expenses accounted for a half of this price. It is well-known that the most influential parameters to minimise the total cost for a GCHP system are the depth and number of boreholes [11]. Indeed, a better thermal performance of the BHE may result in a lower total required BHE length and, as a consequence, a lower total cost.

The borehole thermal resistance is a key performance characteristic as well as a critical design parameter; the lower the thermal resistance, the better the thermal performance of BHE, and the lower the required borehole length [12]. Hence, improving the thermal performance of BHEs is a primary way to support developments of GCHP systems. In this context, several studies have been recently carried out on performance optimisation of BHEs, e.g. thermally-enhanced grouting materials [13], HDPE pipes [14], and working fluid [15], as well as novel configuration of the BHE [16].

In terms of the circuit fluid, the requirement for deep boreholes may be ascribed to the inherently poor thermal conductivity of conventional fluids such as the water and ethylene glycol solution (EGS) that have been used abundantly in GCHP systems due to their availability and low cost. In this context, utilising nanofluids, namely suspension of nanosized particles in the base fluid, would be a promising way to overcome the poor thermal conductivity of conventional working fluids. Numerous studies have investigated the thermal performance of various heat exchangers using nanofluids [17-20] and they have reported the heat transfer enhancement of heat exchangers in presence of nanoparticles.

Recently, several studies have investigated the potential application of nanofluids in geothermal heat pump systems. Sui et al. [21] examined the thermophysical properties of nanofluids for using in geothermal heat pump systems. Their results indicated the importance of viscosity and heat capacity of nanofluids in geothermal energy extraction. Daneshipour and Rafee [22] compared numerically the thermal performance of Al_2O_3- and CuO-water nanofluids in a coaxial borehole. It was shown that CuO nanoparticles render better thermal performance than Al_2O_3 nanoparticles in coaxial boreholes. However, this better thermal performance was at the penalty of higher pressure drop. The stability of nanofluid suspensions in a coaxial BHE during the shut-down process was investigated by Sun et al. [23]. Their numerical results indicated that when the fluid is static, accumulation of nanoparticles appears to be near of the heat exchanger bottom, after many hours of sedimentation. However, the accumulated particles could be removed by the fluid flow at a relatively high velocity. They concluded that nanofluid suspensions show a good stability ensuring their operational reliability in geothermal heat exchangers. Du et al. [24, 25] investigated thermal performance of CuO-water nanofluid in a sand box setting with W-shaped tubes, by means of both numerical simulations and experiments. The obtained results showed that using CuO nanoparticles results in 39.8% enhancement of the heat transfer rates and 16.6% increase in

pumping power. Furthermore, it was shown that the spherical particle-based nanofluid is characterised by 8.5% higher energy efficiency, compared to the rod-shaped one. Kapıcıoglu and Esen [26] evaluated the Al_2O_3-ethylene-glycol/water nanofluid in shallow horizontal ground heat exchangers with U-tube as well as the spiral pipe. Their experimental results showed that the COP of U-type BHE and spiral BHE systems had a 2.5% and 3.0% increase, respectively, by using nanofluid with 0.1% volume fraction. However, the higher volume concentration (0.2%) did not render any performance enhancement.

The literature review shows that there are a limited number of studies concerning the performance of vertical U-tube BHEs utilising nanofluids as the heat transfer fluid. Narei et al. [27] theoretically analysed the effect of employing Al_2O_3-water nanofluid on reducing the BHE length. They tried to optimise the effective thermal conductivity and viscosity of the nanofluid by means of the multi-objective Flower Pollination algorithm. Their results revealed that Al_2O_3-water nanofluid contributed to a reduction less than 1.3% of the bore length, in comparison to pure water as a working fluid. Diglio et al. [28] conducted a comparative numerical study to find the best nanofluid in terms of the highest heat transfer enhancement and the highest reduction in the BHE thermal resistance of a single U-tube BHE. They found that the highest heat exchange rate and the highest reduction in the BHE thermal resistance is associated with the Ag- and Cu-water nanofluids, respectively. Thermal performance of Cu-water nanofluid in single U-tube BHEs was investigated by Jahanbin et al. [29] through finite element simulations. It was revealed that in presence of nanoparticles the borehole thermal resistance is reduced and the BHE renders a better thermal performance, compared to utilising water as a circuit fluid. Javadi et al. [30] by means of numerical simulations investigated the impact of employing hybrid nanofluids on the thermal performance of a shallow vertical U-tube BHE. It was found that all the evaluated hybrid nanofluids present a lower coefficient of performance (COP) compared to the pure water. They concluded that applying the hybrid nanofluids as working fluid is not economically viable because of having higher pressure drop than the heat transfer enhancement.

Several of studies cited above have concluded the applicability of nanofluids in geothermal heat pump systems, however, they have mostly asserted that a more extensive evaluation on performance of different nanofluids under realistic operating conditions is required. In addition, the main focus of these studies has been revolved around the heat transfer enhancement of BHEs

in presence of nanofluids and the simultaneous effects of nanofluids on several influential parameters of GCHP systems have been neglected.

In this context, the present study aims to investigate comprehensively the performance of single U-tube BHEs utilising nanofluids as the circuit fluid. Seven common nanoparticles with a volume fraction ranging from 0.1% to 2.0% have been selected to be evaluated as a heat carrier fluid under different working conditions. Several performance indicators are introduced and the performance of various nanofluids are examined through a series of 3D finite element simulations. Firstly, a comparative techno-economic analysis is performed to highlight the merits and drawbacks of each nanofluid, with respect to pure water, in GCHP systems. Then, a sensitivity analysis is performed in order to optimise the decrement percentage of the BHE thermal resistance and outlet fluid temperature in presence of nanofluids. Finally, by means of the linear regression of 3D simulation results obtained for different nanofluids, simple equations are proposed allowing evaluation of the outlet fluid temperature for single U-tube BHEs utilising nanofluids as a working fluid. Findings of the present study are expected to provide an insight into potential application of nanofluids in GCHP systems.

2. Methods

2.1. Physical model

The geometry under study is a single U-tube BHE consisting of the HDPE pipe and sealing grout, surrounded by the ground. The ground around the BHE was modelled as a cylinder coaxial with the borehole, with diameter of 10 m and a length 10 m longer than that of the BHE. Sketch of the BHE cross section is illustrated in Fig. 1(a), where D_b, D_e, D_i, and s refer to the BHE diameter, outer diameter of pipe, inner diameter of pipe, and shank spacing, respectively.

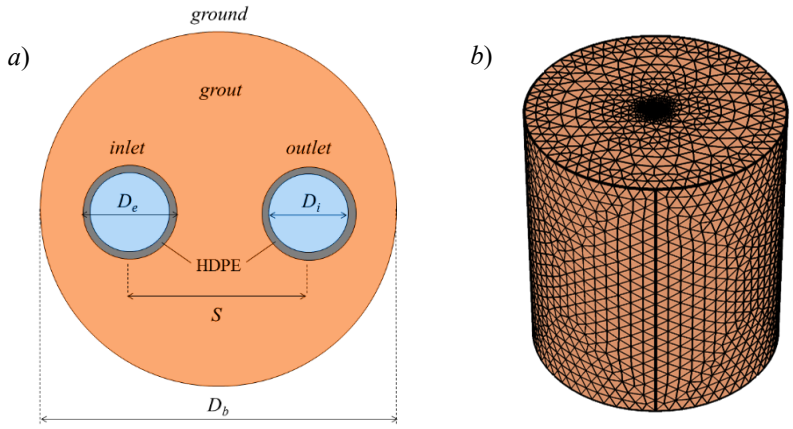

Fig. 1. Sketch of the BHE cross section (a) and illustration of the adopted mesh (b).

In the present study, various values of thermophysical properties as well as different physical arrangements of the BHE components were considered for numerical simulations. Table 1 reports the summary of adopted values for the thermophysical properties, geometric parameters and operating conditions. For the baseline simulations, a customary BHE with intermediate parameters and properties were regarded, namely L=100 m, D_b=16 cm, D_e=40 mm, D_i=32.6, s=95 mm, $\dot{V}$=15 l/min, k_{gd}=1.8 W/(m.K), and k_{gt}=1.6 W/(m.K).

Table 1. Summary of adopted thermophysical properties, geometric parameters and operating conditions.

Parameter	Value
BHE length (L)	50, 100, 150, 200 m
BHE diameter (D_b)	15, 15.5, 16, 16.5, 17 cm
Inner pipe diameter (D_i)	31.4, 32.0, 32.6, 33.4, 34.0 mm
External pipe diameter (D_e)	38.8, 39.4, 40.0, 40.8, 41.4 mm
Shank spacing (s)	85, 90, 95, 100, 105 mm
Surrounding ground diameter	10 m
Ground thermal conductivity (k_{gd})	1.6 - 2.4 W/(m.K)
Grout thermal conductivity (k_{gt})	1.2 - 2.1 W/(m.K)
HDPE thermal conductivity (k_p)	0.5 W/(m.K)
Heat capacity per unit volume of ground $(\rho c_p)_{gd}$	2.500 MJ/(m^{3}K)
Heat capacity per unit volume of grout $(\rho c_p)_{gt}$	1.600 MJ/(m^{3}K)
Heat capacity per unit volume of HDPE $(\rho c_p)_p$	1.824 MJ/(m^{3}K)
Operating mode	Cooling
Operating duration	100 h
Ambient temperature	24 ºC
Inlet temperature (T_{in})	30 ºC
Volume Flow rate ($\dot{V}$)	10, 15, 20, 30 l/min

Process of the whole analysis conducted in the present study, including different steps for the numerical modelling, simulation and post-processing of the results is demonstrated in Fig.2

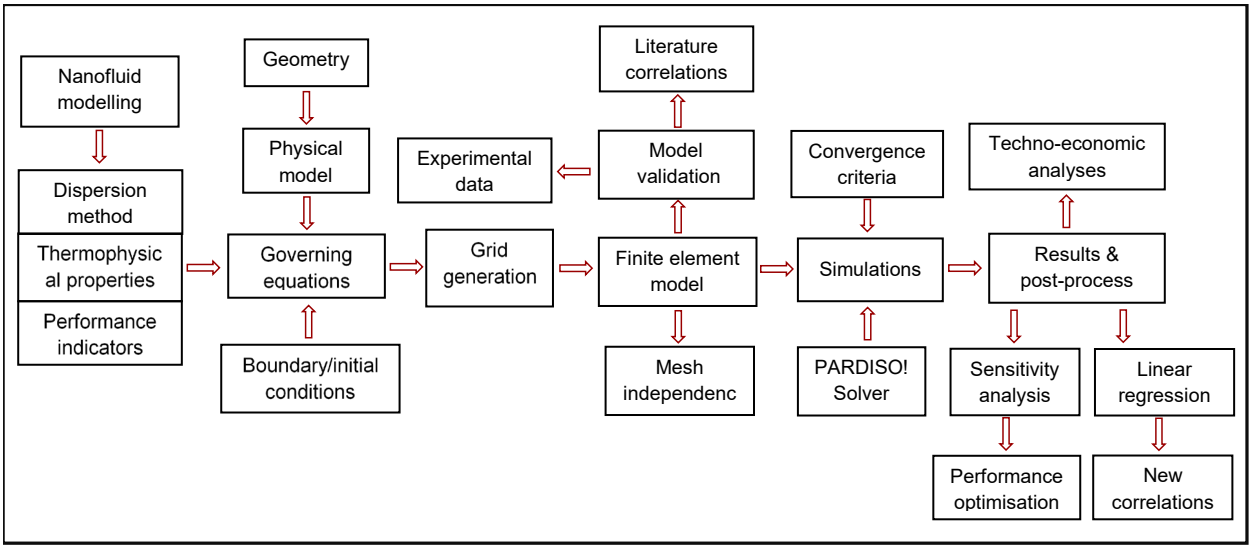

Fig. 2. A flow chart describing the structure of the present study.

2.2. Numerical method

A similar numerical code to that employed in a previous study [31] was adopted, which is briefly described here. A 3D transient finite element code, implemented through COMSOL Multiphysics software, was developed to solve the conjugate heat transfer problem for an operating duration of 100 h. The selected operation period was more than adequate to reach a steady-flux heat transfer regime.

The computational domain consists of three solid domains, namely the HDPE pipes, sealing grout, and ground, along with a fluid domain inside the U-loop. The heat is rejected from the fluid to the internal surface of the tube by means of convective heat transfer, whereas it transfers subsequently through the HDPE, grouting material and ground by conduction. Continuity of the heat flux and temperature was assumed between the pipes and the grout, and between the BHE and the surrounding ground. The equality of boundary temperatures was also imposed as a coupling condition. The corresponding governing equations of the computational domain can be found in Ref. [31], which is not presented here for the sake of brevity. The time-dependent "PARDISO" solver with non-uniform time steps was utilised to solve the transient heat transfer problem with the relative and absolute tolerance equal to 10^{-3} and 10^{-4}, respectively.

The summer-cooling condition was considered and the water as well as various nanofluids were regarded as heat carrier fluids. It was assumed that the fluid flows with uniform velocity in the vertical direction with corresponding volume flow rate (Table1). Values of the thermophysical properties of water were taken from NIST [32], and were evaluated at the reference inlet temperature, namely T=30 ºC.

As a boundary condition, the bottom and lateral surfaces of the ground were considered as adiabatic. The external boundary of the computational domain, i.e. the surface at z = 0 of the BHE, was considered as adiabatic, while that of the ground was assumed to be isothermal equal to the ambient temperature, i.e. 24 °C. As an initial condition, the temperature was set equal to the undisturbed ground temperature, for both the BHE and the ground. The undisturbed ground temperature was assumed to be 14 °C at a depth z=10 m, increasing with a geothermal gradient of 0.03 °C per meter for z > 10 m. For z < 10 m, an exponential change of the ground temperature with depth was considered [33], namely:

$$\begin{cases} T_{gd}(z) = T_{gd}(10) + \left[T_{gd}(0) - T_{gd}(10) \right] \times e^{-z} & 0 \le z \le 10 \text{ m} \\ T_{gd}(z) = 14 + 0.03 \times z & z > 10 \text{ m} \end{cases} \quad (1)$$

The mean value of T_{gd} between 0 and 100 m and between 0 and 200 m turned out to be 15.31 °C and 16.75 °C, respectively.

For each geometry, including different values of the BHE's diameter, length and shank spacing, the computational domain was meshed with unstructured tetrahedral elements. A mesh with higher density was applied in fluid region as well as the solid-fluid interface while a smoother mesh with expansion rate was regarded for the far-field solid regions. The selected mesh for baseline simulations with L=100 m, d_b=160 mm and s=95 mm consists of 1,478,175 tetrahedral elements, varying to some extent with alterations in the BHE configuration and length. The selected mesh for the baseline simulations is illustrated in Fig. 1(b).

Table 2. Mesh independence of the results.

Mesh No.	Elements	T_{out} (°C)	Deviation from Mesh 3 [%]	q_l (W/m)	Deviation from Mesh 3 [%]
1	1,241,509	26.041	0.23	40.321	0.94
2	1,354,423	25.948	0.12	41.024	0.79
3	1,478,175	25.981	-	40.701	-
4	1,587,856	26.017	0.14	40.957	0.62
5	1,633,404	25.969	0.05	40.870	0.42

The mesh independence of the results was ensured by performing preliminary computations with five different meshes. Mesh independence check was performed for a BHE with L=100 m and s=95 mm, in the following conditions: T_{in}=30 °C, $\dot{V}$=15 l/min, k_{gt}=1.6 W/(mK) and k_{gd}=1.8 W/(mK). Table 2 compares values of T_{out} and q_l obtained by different meshes as well as their corresponding discrepancy from the selected mesh, namely Mesh 3. The table shows that the results obtained by different meshes are nearly coincident. The maximum percent deviation of results from the Mesh 3 is 0.23% for T_{out} and 0.94% for q_l, indicating the mesh independence of the results.

2.3. Modelling of nanofluids

For modelling the nanofluids in ground heat exchangers, it has been a common practice to assume that ultrafine nanoparticles can be easily dispersed in the host fluid, i.e., both the nanoparticles and base fluid are considered to be in thermal balance without any slip between their molecules (homogeneous liquid). However, the nanofluid suspension is inherently a two-phase fluid and slip motion between liquid molecules and solid particles is not negligible. In fact, this random movement of nanoparticles ameliorates the thermal dispersion in nanofluid suspension. In the present study, the thermal dispersion model [34] was employed for the heat transfer modelling of nanofluids. It is assumed that irregular and random movements of nanoparticles induce small perturbation in both temperature and velocity terms, denoted by T' and $\vec{u}'$. Therefore, the intrinsic phase averages are given as:

$$T = \langle T \rangle^{bf} + T' \; ; \qquad \vec{u} = \langle \vec{u} \rangle^{bf} + \vec{u}' \tag{2}$$

where

$$\langle T \rangle^{bf} = \frac{1}{V_{bf}} \int_{V_{bf}} T \, dV + T' \; ; \qquad \langle \vec{u} \rangle^{bf} = \frac{1}{V_{bf}} \int_{V_{bf}} \vec{u} \; dV + T' \; ; \qquad \frac{1}{V_{bf}} \int_{V_{bf}} T' dV = 0 \tag{3}$$

where subscript *bf* refers to the base fluid. By assuming that the boundary layer between the fluid and nanoparticles is negligible, the energy balance equation is expressed as:

$$\left(\rho c_p\right)_{nf} \left[\frac{\partial \langle T \rangle^{bf}}{\partial t} + \langle \vec{u} \rangle^{bf} . \nabla \langle T \rangle^{bf} \right] = \nabla . \left(k_{nf} \nabla \langle T \rangle^{bf} \right) - \left(\rho c_p\right)_{nf} \nabla \left\langle \vec{u}' \; T' \right\rangle^{bf} \tag{4}$$

Also, the heat flux induced by the thermal dispersion in nanofluid flow, q_d, is given by:

$$q_d = \left(\rho c_p\right)_{nf} \langle \vec{u}' T' \rangle^{bf} = -\mathbf{k}_d \; . \nabla \langle T \rangle^{bf} \tag{5}$$

where $\mathbf{k}_d$ is the tensor of thermal conductivity due to the thermal dispersion and subscript *nf* refers to nanofluid. Substituting Eq. (5) in Eq. (4) yields:

$$\frac{\partial \langle T \rangle^{bf}}{\partial t} + \langle \vec{u} \rangle^{bf} . \nabla \langle T \rangle^{bf} = \nabla . \left[\left(\alpha_{nf} \mathbf{I} + \frac{\mathbf{k}_d}{\left(\rho c_p\right)_{nf}} \right) . \nabla \langle T \rangle^{bf} \right] \tag{6}$$

where α is thermal diffusivity and **I** is the identity tensor. The effective thermal conductivity of nanofluids and the Nusselt number take the following forms:

$$k_{eff} = k_{nf} + k_d \tag{7}$$

$$Nu_{nf} = \frac{h_{nf} D_i}{k_{eff}} \tag{8}$$

The dispersed thermal conductivity k_d is calculated through following equation [35]:

$$k_d = \varphi (\rho c_p)_{nf} \, c^* r_p \, u_m \tag{9}$$

where φ is the volumetric fraction of nanofluids, c^* is an empirical constant, r is the pipe radius and u_m is the average bulk velocity of nanofluid.

The thermal conductivity of nanofluids can be obtained by employing the following equation proposed by Yu and Choi [36]:

$$k_{nf} = k_{bf}\left[\frac{k_{np} + 2k_{bf} + 2\varphi(k_{np} - k_{bf})(1+\beta)^3}{k_{np} + 2k_{bf} - \varphi(k_{np} - k_{bf})(1+\beta)^3}\right] \tag{10}$$

where subscript *np* refers to nanoparticles and β is the ratio of the nanolayer thickness to the original particle radius and is considered equal to 0.1.

The density of nanofluid is obtained by using the correlation proposed by Pak and Cho [37], defined as follows:

$$\rho_{nf} = \varphi\rho_{np} + (1-\varphi)\rho_{bf} \tag{11}$$

The specific heat of nanofluids is calculated by the model proposed by Xuan and Roetzel [34] based on the heat equilibrium model:

$$c_{p,nf} = \frac{\varphi\left(\rho c_p\right)_{np} + (1-\varphi)\left(\rho c_p\right)_{bf}}{\varphi\rho_{np} + (1-\varphi)\rho_{bf}} \tag{12}$$

The viscosity of nanofluids is calculated by the model of Wang et al. [38]:

$$\mu_{nf} = \left(1 + 7.3\varphi + 123\varphi^2\right)\mu_{bf} \tag{13}$$

In the present study, seven different nanofluids have been selected to be evaluated as the heat carrier fluid. The volume fraction of nanofluids, φ, has been considered in the range of 0.1% to 2.0%. Table 3 reports the thermophysical properties of different nanoparticles as well as the base fluid regarded in this study.

Table 3. Thermophysical properties of the base fluid and nanoparticles [28, 30].

Thermal properties	Base fluid	Nanoparticle						
	Water	Cu	Ag	Al_2O_3	Fe_2O_3	SiO_2	CuO	TiO_2
ρ (kg/m^3)	995.03	8933	10490	3900	5210	2260	6500	4175
c_p (J/(kg.K)	4179.8	385	235	880	637	1050	525	692
k (W/(m.K)	0.6155	401	450	41	7.9	148	32.9	8.4

2.4. Performance indicators

To address comprehensively the applicability and performance of various nanofluids in GCHP systems, different performance indicators in this study have been considered to be evaluated. In terms of the thermal performance, the Mouromtseff Number (*Mo*), BHE thermal resistance and BHE effectiveness coefficient are evaluated as figure of merit for heat transfer of nanofluids. The Mouromtseff Number (*Mo*) evaluates the effects of fluid properties on the convective heat transfer coefficient of the circuit fluid; a higher *Mo* indicates a better heat transfer capability of the circuit fluid. The *Mo* is a function of the density, viscosity, thermal conductivity and specific heat and is expressed by: [39]

$$Mo = \frac{\rho^{0.8} k^{0.67} c_p^{\ 0.33}}{\mu^{0.46}} \tag{14}$$

To evaluate the effect of different nanoparticles on the borehole thermal resistance, the decrement percentage of thermal resistance with respect to the base fluid is studied, denoted as ΔR_b, and is defined as:

$$\Delta R_b = \frac{R_{b,bf} - R_{b,nf}}{R_{b,bf}} \times 100 \tag{15}$$

The borehole thermal resistance, R_b, is obtained by [40]:

$$R_b = \frac{T_m - T_b}{q_l} \tag{16}$$

where T_m is the mean fluid bulk temperature, T_b is the mean temperature of the external surface of the borehole, and q_l is the mean heat flux per unit of BHE length. T_m is determined as:

$$T_m = \frac{1}{2L}\left(\int_0^L T_d(z)dz + \int_0^L T_u(z)dz \right) \tag{17}$$

where T_d and T_u are bulk temperatures of the descending fluid and of the ascending fluid, respectively.

The BHE effectiveness coefficient, ε, is defined as the ratio of the actual heat transfer to and from the BHE, for a given inlet temperature, to the maximum possible theoretical heat transfer between

the circuit fluid and the surrounding ground [41]. Effectiveness coefficient is a dimensionless factor, varying from 0 to 1, and is given by:

$$\varepsilon = \frac{\dot{Q}_{actual}}{\dot{Q}_{\max}} = \frac{\dot{m}c_p(T_{in} - T_{out})}{\dot{m}c_p(T_{in} - T_{gd})} \tag{18}$$

In order to analyse the effect of nanofluids on the pressure drop and, consequently, on the required pump power, the pumping power W_p is evaluated as:

$$W_p = \frac{\dot{m}}{\omega_p \rho} \Delta P \tag{19}$$

where $\dot{m}$, ΔP, and ω_p are the mass flow rate (kg/s), pressure drop (Pa) and the pump efficiency, respectively. The increment percentage of the pumping power, with respect to the base fluid, is estimated by:

$$\Delta W_p = \frac{W_{p,nf} - W_{P,bf}}{W_{p,bf}} \times 100 \tag{20}$$

To address the combined effects of the heat transfer and pressure drop in presence of nanoparticles, the COP improvement factor (η) is considered. The COP improvement factor is a useful index in which values of η greater than unity (η >1) indicate the efficiency of nanofluids in terms of the heat transfer and pressure drop, i.e. higher rate of the heat transfer enhancement than the pressure drop. It is expressed as [42]:

$$\eta = \left(\frac{Nu_{nf}}{Nu_{bf}}\right)\left(\frac{f_{bf}}{f_{nf}}\right)^{0.333} \tag{21}$$

where f refers to the friction factor, and for the base fluid (water) and nanofluids can be given by [43]:

$$f_{bf} = \frac{0.3164}{Re^{0.25}} \tag{22}$$

$$f_{nf} = \frac{0.3164}{Re^{0.25}}\left(\frac{\rho_{nf}}{\rho_{bf}}\right)^{0.797}\left(\frac{\mu_{nf}}{\mu_{bf}}\right)^{0.108} \tag{23}$$

Equation (22) is the Belasius correlation for a turbulent single-phase pipe flow, valid for $Re_{tr}<Re<10^5$, and Eq. (23) is the modified version of the Eq. (22) for nanofluids.

The percentage of possible reduction in the borehole length in presence of nanofluids is estimated by [44]:

$$\Delta L = m_{nf} c_{p,nf} \frac{\theta}{q_l L_{bf}} \times 100 \tag{24}$$

where θ is the difference between the outlet fluid temperature (T_{out}) of base fluid and nanofluid, namely:

$$\theta = T_{out,bf} - T_{out,nf} \tag{25}$$

In addition, the decrement percentage of the outlet fluid temperature with respect to the base fluid is calculated by:

$$\Delta\theta = \frac{(T_{out,bf} - T_{out,nf})}{T_{out,bf}} \times 100 \tag{26}$$

Regarding the economic analysis, the cost of GCHP systems employing nanofluids increases not only because of the increase of pressure drop and therefore a higher power consumption of the circulation pump, but also due to the capital cost of nanoparticles. The cost of nanofluids in GCHP systems can be estimated as [45]:

$$Cost = C_{np} + C_{el} + C_{other} \tag{27}$$

where C_{np} is the capital cost of nanoparticles, C_{el} is the cost of electrical energy, and C_{other} is additional costs including variable costs related to the preparation of the nanofluid as well as the maintenance costs. The additional costs may change considerably depending on the preparation and stabilisation methods and operational conditions of the system and are disregarded in this study. Hence, the capital cost of nanoparticles, C_{np}, and the cost of electrical energy C_{el} can be considered as the main costs of the system in presence of nanofluids. The capital cost of nanoparticles per unit length of borehole can be calculated as [46]:

$$C_{np} = \frac{\varphi \rho_{np} V_{nf} . C_{s,np}}{L} \tag{28}$$

where ρ_{np} is the density of nanoparticles, V_{nf} is the volume of nanofluid, and $C_{s,np}$ is the specific cost of nanoparticles in €/kg according to the market price. The purchase costs of nanoparticles ($C_{s,np}$) have been regarded on the basis of recently observed market prices. However, it should be noted that these prices would drastically differ depending on their preparation, size, purity, etc. Values of the specific cost employed in this study for different nanoparticle are reported in Table 4.

Table 4. Specific cost of nanoparticles [47].

	Al_2O_3	Ag	Cu	CuO	Fe_2O_3	SiO_2	TiO_2
C_s (€/g)	0.26	9.74	1.23	0.34	0.19	0.31	0.23

The cost of electrical energy, C_{el}, can be calculated as follows [28]:

$$C_{el} = \frac{\Delta P \, \dot{V}_{nf} \, t}{\omega_p} C_{s,el} \tag{29}$$

where $\dot{V}_{nf}$ is the volume flow rate of nanofluids, t is the operation time in hour, and $C_{s,el}$ is the specific cost of electrical energy given in € / kWh. The specific cost of electrical energy, $C_{s,el}$, has been adopted based on the average specific cost in European Union for the first half of 2021 [48], which is equal to 0.2322 € / kWh.

3. Model validation

To validate the employed numerical model for BHE simulations, the time evolution of outlet fluid temperature yielded by numerical simulation is compared with those obtained by Jalaluddin et al. [49] through experiments, illustrated in Fig 3. The experimental setup consists of a single U-tube BHE with D_b=0.1298 m and L=20 m that installed in a steel case with thickness of 5 mm and the same length as the BHE, sealed by silica sand with thermal conductivity of 1.4 W/(m.K). The U-tube made of polyethylene pipe with D_e=33 mm, D_i=26 mm, and shank spacing of s=53 mm was considered. The volume flow rate was $\dot{V}$=2 *l*/min with an inlet fluid temperature equal to T_{in}=27 °C. The experiments were performed for 24 h of continuous operation under summer-cooling condition. More details on the experimental conditions and thermal properties of materials can be found in Ref. [49]. The utilised numerical method for model validation is identical to that reported in section 2.

The numerical results for very first minutes of the operation were not presented here in order to enhance the readability of the chart. The figure shows that the outlet temperature is an increasing function of time under cooling condition and that the simulated results are in fair agreement with experimental data. The root-mean-square-deviation (RMSD) of numerical results from experimental data is 0.124 °C, equal to normalised-RMSD of 4.87 %, implying the accuracy of employed model.

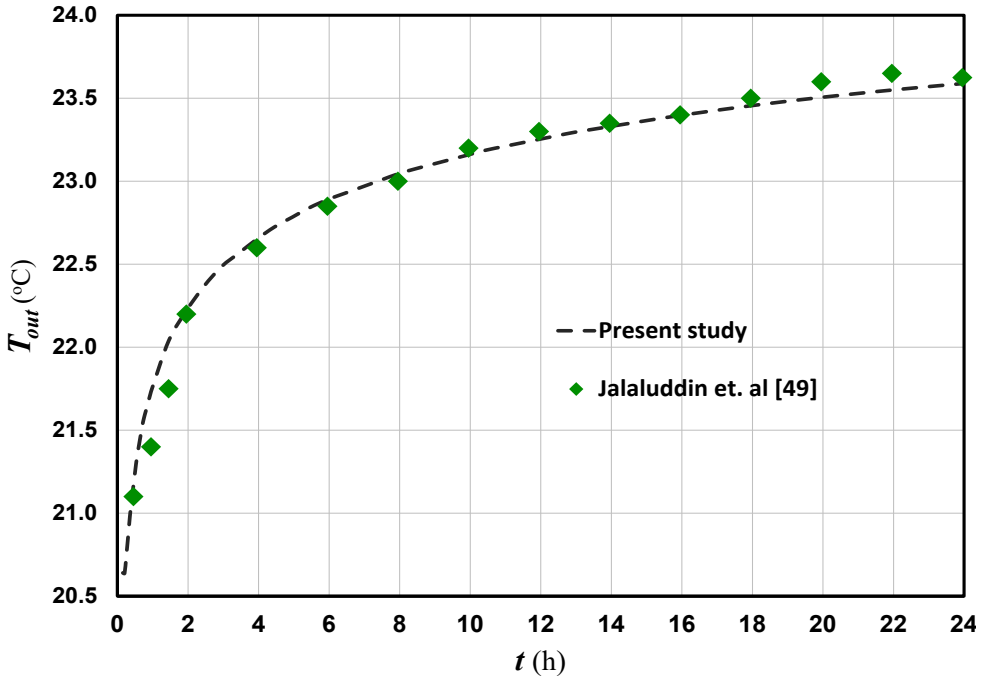

Fig. 3. Comparison of the simulated outlet fluid temperature with experimental data [49].

Another model validation was also carried out in order to show the accuracy of numerical model in simulation of nanofluids. Figure 4 compares values of the Nusselt number (*Nu*) obtained by the present study with those yielded through different correlations available in the literature for nanofluids [37,50-52]. Comparisons were made for a Cu-water nanofluid with an intermediate volume fraction, namely φ=0.5%, at four different volume flow rates. The figure shows that by increasing the volume flow rate, the Nusselt number enhances and that the discrepancy between various models in prediction of Nusselt number increases. Nonetheless, the results yielded by the numerical model do not exceed the upper or lower thresholds, for any volume flow rate.

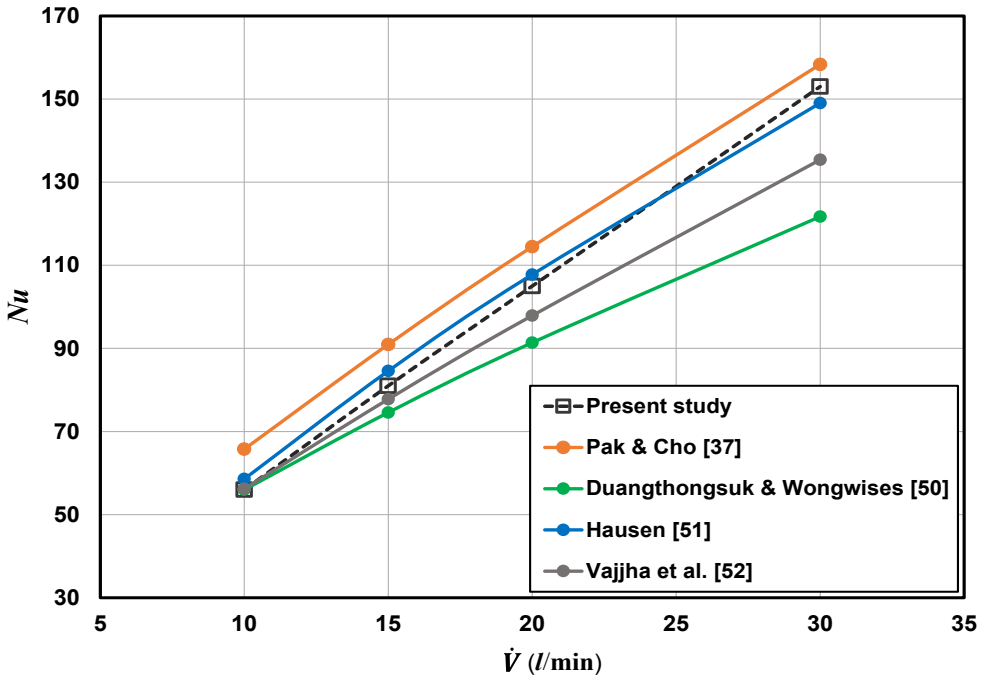

Fig. 4. Comparison of the Nusselt number: Present study vs. available correlations in the literature.

4. Results and discussion

4.1. Performance evaluation of nanofluids

Figure 5 compares the normalised nanofluid *Mo* number with respect to water for various nanofluids. The *Mo* number examines the effects of fluid properties on the convective heat transfer and its greater value indicates a better thermal performance. The figure shows that the convective heat transfer rate augments by increasing the volume fraction of nanofluids. It is evident from the figure that the Ag- and Cu-based nanofluids are characterised by the highest *Mo* number in any volume fraction (up to 14%). On the other hand, SiO_2 nanoparticle followed by TiO_2 show the lowest heat transfer enhancement among different nanofluids (less than 0.75%). The figure indicates that the difference between Mo^* of different nanofluids is insignificant when the volume fraction is lower than 0.5%, whereas by increasing the nanofluid fraction, the impact of nanofluid type on the heat transfer enhancement becomes more striking.

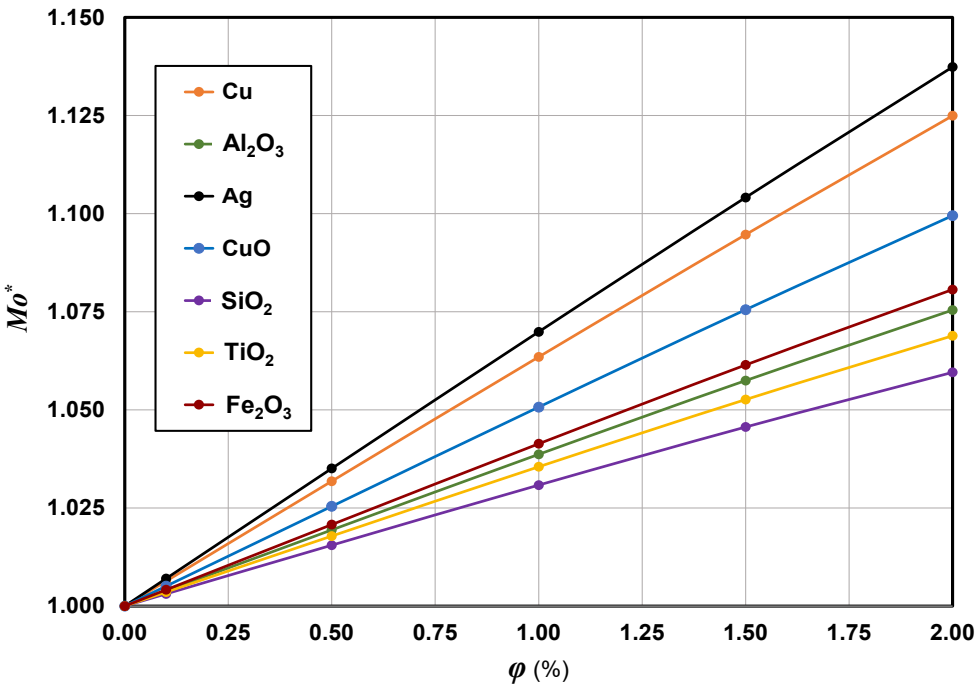

Fig. 5. Comparison of the normalised *Mo* number for different nanofluids.

Since nanoparticles affect the convective resistance film, it can be expected that those nanofluids showed a greater *Mo* number be characterised by a higher decrease in the borehole thermal resistance. Table 5 reports the decrement percentage of thermal resistance, ΔR_b, for different nanofluids. The results indicate an average increment of 2% in ΔR_b for all nanofluids by increasing φ from 0.1% to 2.0%. However, it should be noted that reported values of ΔR_b in Table 5 correspond to a borehole with specific characteristics. In section 2 of the results, we examine influential parameters along with the nanofluid fraction in order to find conditions in which the optimum ΔR_b for nanofluids can be obtained.

Table 5. The decrement percentage of thermal resistance (ΔR_b) by volume fraction for different nanofluids.

	ΔR_b (%)						
φ (%)	Cu	Al_2O_3	Ag	CuO	SiO_2	TiO_2	Fe_2O_3
0.1	0.38	0.38	0.38	0.38	0.37	0.37	0.37
0.5	1.20	1.15	1.21	1.17	1.13	1.15	1.16
1.0	1.78	1.74	1.81	1.77	1.69	1.74	1.75
1.5	2.19	2.13	2.23	2.16	2.09	2.13	2.14
2.0	2.48	2.41	2.52	2.44	2.37	2.40	2.42

The increment percentage of the pumping power (ΔW_p) in presence of nanofluids, with respect to water as base fluid, is compared in Fig. 6 for different nanofluid fractions. Unlike the thermal performance of nanofluids (Fig. 5 and Table 5), the results indicate that Ag and SiO_2-based nanofluid are the worst and the best cases respectively, in terms of the required pumping power, for any nanofluid fractions. It can be observed that for φ=2.0%, the Ag-water nanofluid requires 27% and 21% more pumping power, compared to SiO_2- and Al_2O_3-based nanofluids, respectively. A comparison between results of Fig. 6 and Table 3 implies that a higher density of nanoparticle is associated with a higher required pumping power. The chart also shows that ΔW_p significantly increases as the volume fraction of nanofluids grows, which can be explained by the proportional relation of the pumping power to the mass flow rate and the pressure drop, according to Eq. (19). Indeed, the density of nanofluids increases linearly with volumetric concentration and, consequently, results in increase of the mass flow rate as well as the pressure drop, for a given volume flow rate. It is noteworthy to mention that the increase in pressure drop of different nanofluids, with respect to pure water, is characterised by the same trend as ΔW_p.

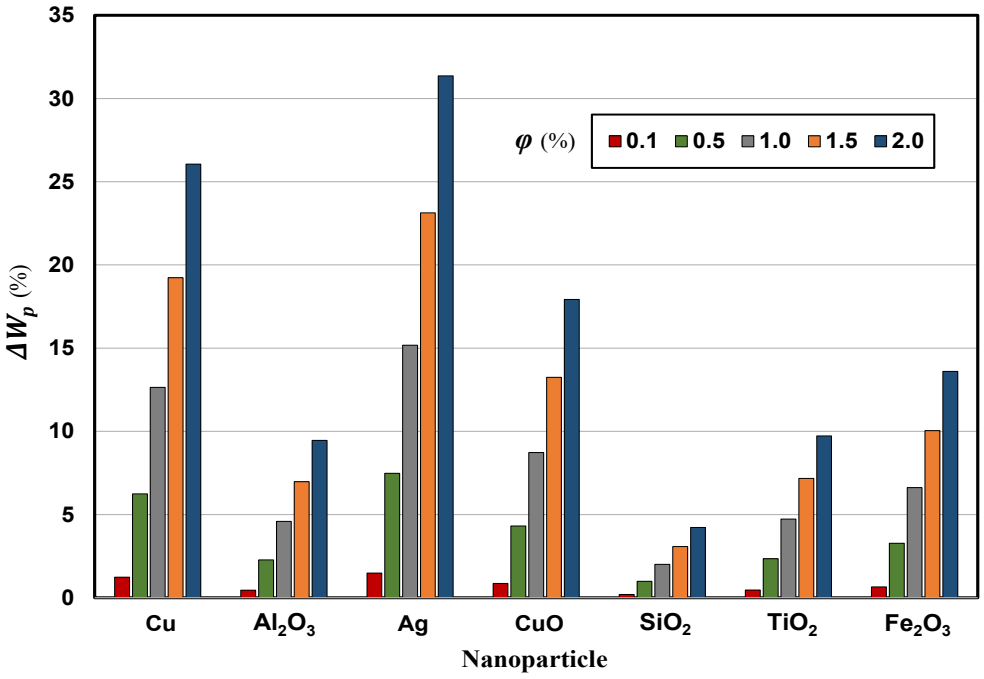

Fig. 6. The increment percentage of the pumping power (ΔW_p), with respect to pure water, for various nanofluids.

For different nanofluids, Fig. 7 demonstrates the COP improvement factor (η), which evaluates the combined effects of the heat transfer and pressure drop. Values greater than unity, η >1,

indicate the effectiveness of nanofluids in terms of the heat transfer and pumping energy consumption. The figure shows that values of η increase with volume fraction in a semi parabolic trend and the results confirm the efficiency of regarded nanofluids in terms of the COP improvement factor over different volume fractions. Comparing Figs. 5 and 7 shows that the order of most preferable nanofluids in terms of the COP improvement factor is similar to that for *Mo* number, except TiO_2-based nanofluid that renders a slightly higher η than Al_2O_3-based one. It can be observed that for values φ lower than 0.5%the difference between corresponding values of η for different nanofluids is negligible, similar to the trend of Fig. 5.

In fact, the presented COP improvement factor (η) in this study can be considered as proportional to the performance efficiency coefficient (PEC) [53], defined as the ratio of heat load-to-pumping power of the nanofluid to base fluid. Du et al. [25] examined in the sand box experiment the time evolution of PEC for a CuO-water nanofluid at the volumetric concentration about 0.5%. Their results showed that the value of PEC for quasi-stationary regime is between 1.15 and 1.25, which is similar to our results yielded for CuO-based nanofluid at φ=0.5%, namely η=1.19.

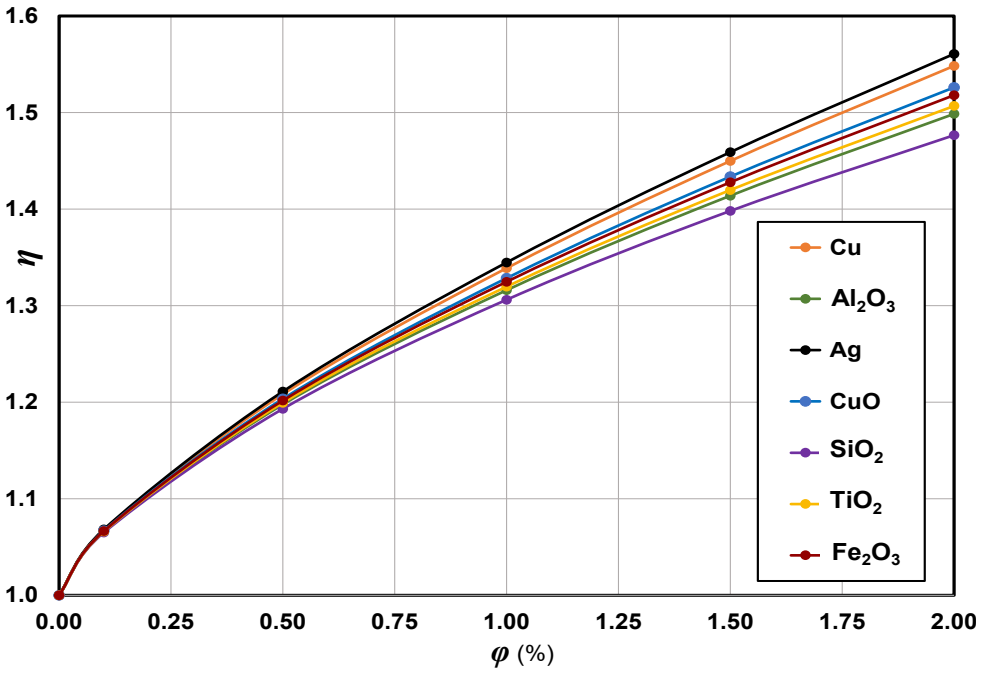

Fig. 7. Comparison of the COP improvement factor (η) for different nanofluids.

Figure 8 compares the percentage of possible reduction in the borehole length (ΔL) and the normalised effectiveness ($\varepsilon^*=\varepsilon_{nf}/\varepsilon_{bf}$) for various nanofluids. Both indicators are a function of the

outlet fluid temperature and the resultant of θ, namely the difference between the outlet fluid temperature of base fluid and nanofluid (cooling operating). The figure shows that the variation trend of ΔL for each nanofluid is quite similar to that of ε^*. The Ag-water nanofluid with 1.52% at φ=2.0%, followed by SiO_2- and TiO_2-based nanofluids, show the highest values of ΔL for any volume fraction among different nanofluids. For the same fraction, the lowest reduction in the BHE length is equal to 1.03% and belongs to the Fe_2O_3-water nanofluid. It is noticeable that the results obtained for the case of Al_2O_3 at φ=2.0, i.e. ΔL=1.12 %, is very close to that reported in the study of Narei et al. [27], namely 1.26%. The elaboration of the numerical results showed that when the average thermal power per BHE unit length increases, ΔL improves to some extent. Nevertheless, it is evident from the results that employing nanofluids as a heat carrier fluid is not promising for the purpose of reducing the borehole length.

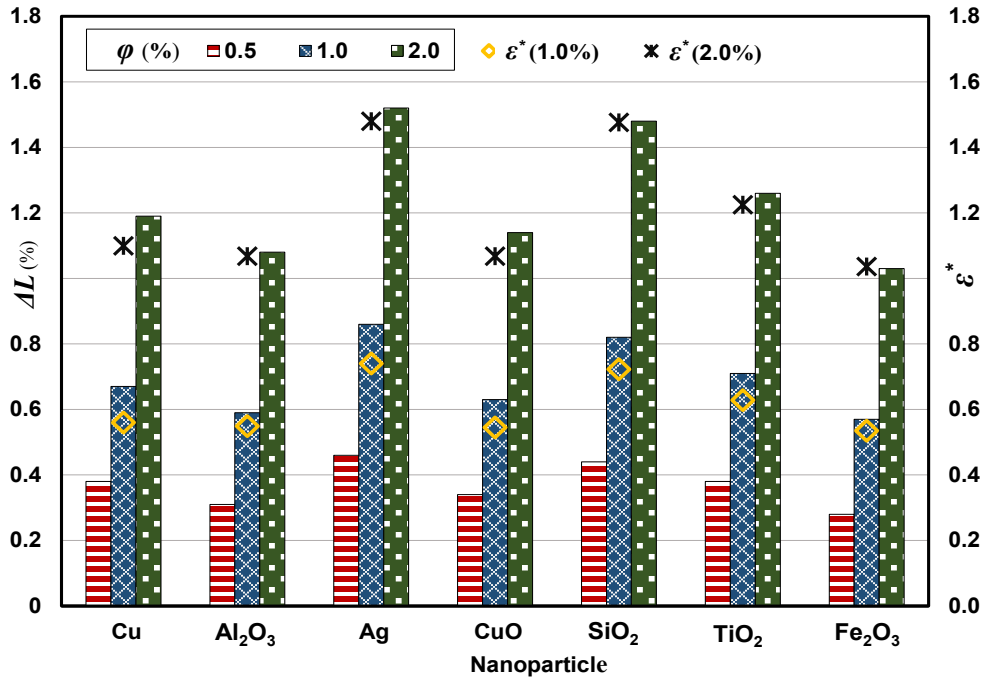

Fig. 8. Comparison of the decrement percentage of borehole length (ΔL) and the normalised effectiveness for different nanofluids.

Regarding the economic analysis, Fig. 9 compares the cost of electrical energy (C_{el}) for two nanofluid fractions at various volume flow rate. The figure shows that while the increase of nanofluid fraction has a minor effect on the cost increment, the volume flow rate can play an important role in the electricity cost. Indeed, increasing the flow rate increases the pressure drop and consequently the pumping power. Among different nanofluids, those demonstrated a higher required pumping power in Fig. 6, namely Ag- and CU-based nanofluids, also here cause a higher

cost of electrical energy. However, the price difference between various nanofluids is insignificant in both nanofluid fractions (less than 2 €/month).

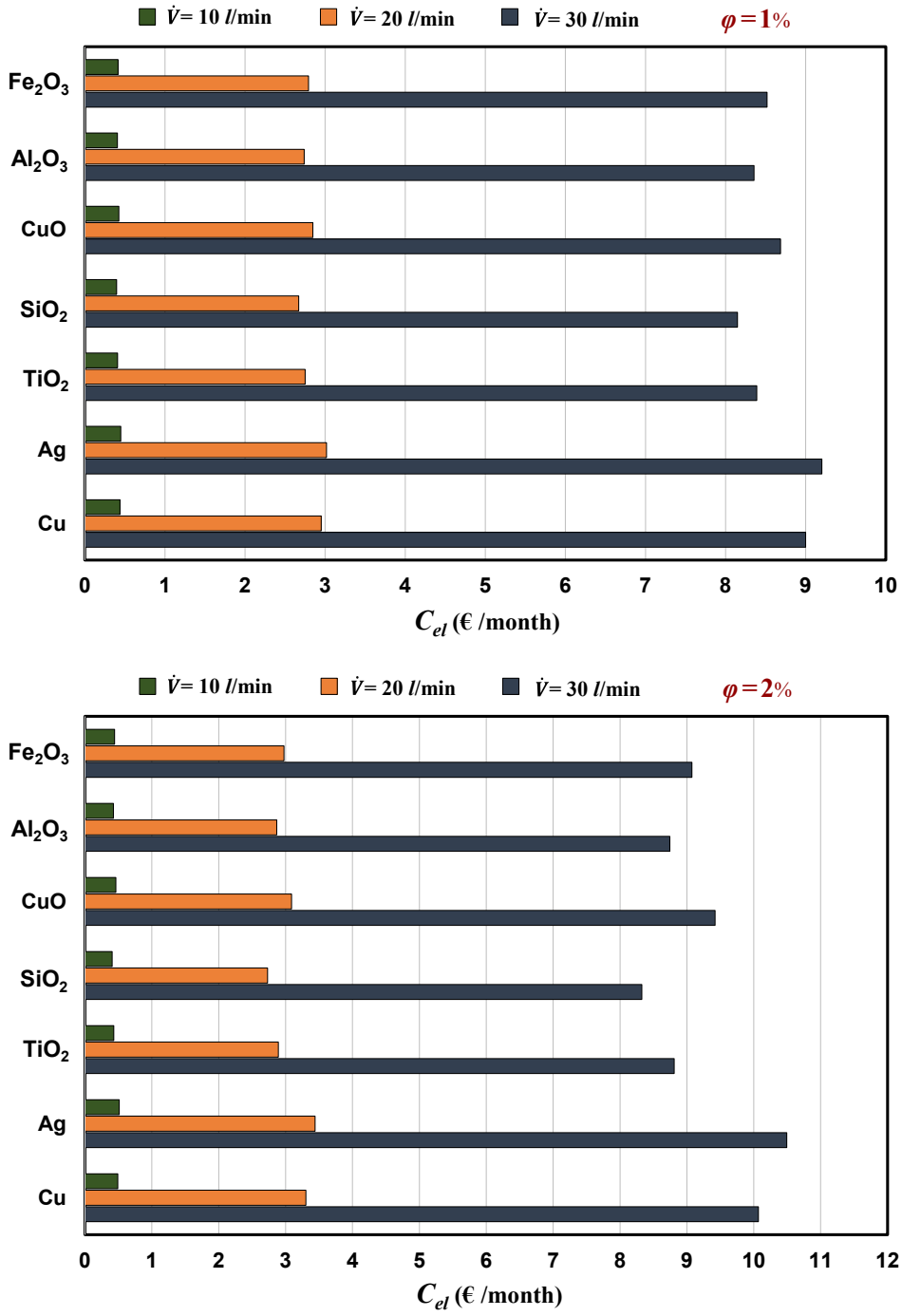

Fig. 9. Electrical energy cost for different nanofluids: φ =1.0% (a) and φ =2.0% (b).

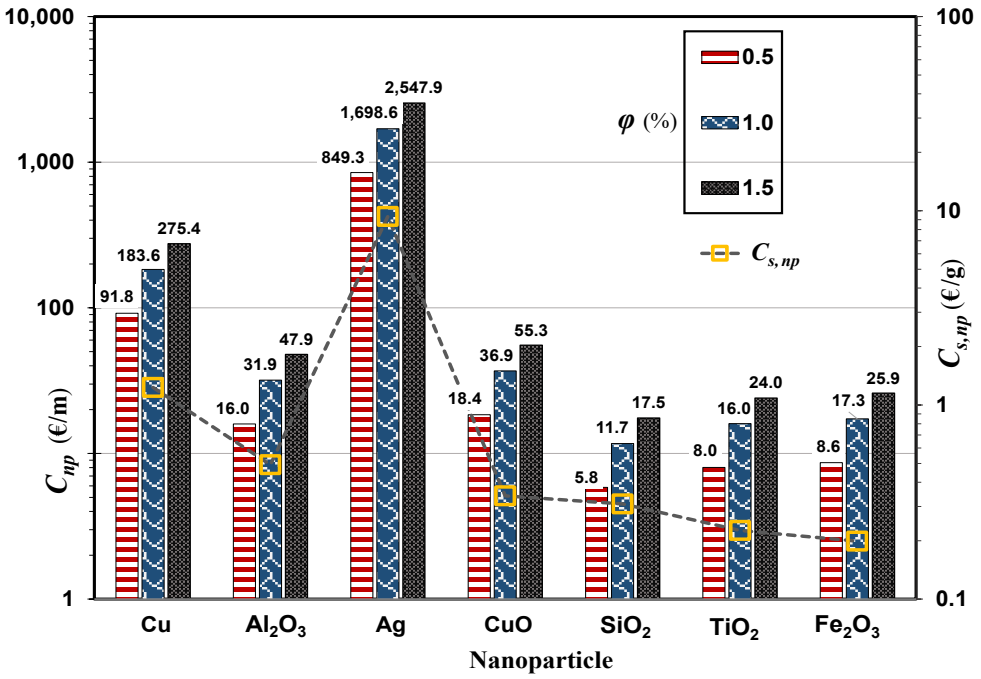

Fig. 10. Capital and specific costs of different nanoparticles for three nanofluid fractions: φ =0.5, 1.0 and 1.5%.

Figure 10 compares the capital and specific cost of different nanoparticles for three nanofluid fractions, i.e. φ=0.5, 1.0 and 1.5%. In order to demonstrate better the comparison between costs of different nanoparticles, values of vertical axes are presented in the logarithmic scale. The figure shows that the capital cost of nanoparticles varies linearly with the volume fraction. The Ag-based nanofluid is by far the most expensive nanoparticle, ranging from about 850 to 2550 €/m, while the SiO_2-based one is the cheapest one, costing between 5.8 and17.5 €/m. It can be observed that, for a given nanofluid concentration, a higher specific cost does not necessarily mean a higher capital cost (see SiO_2 and TiO_2, or Al_2O_3 and CuO). In fact, the combined impact of the specific cost (Table 4) and nanoparticle density (Table 3) is determinant for the capital cost of nanofluids.

Comparisons between Figs. 9 and 10 imply that the cost of electrical energy for nanofluids due to the higher pump consumption is negligible compared to the capital cost of nanoparticles. Assuming the capital cost of the water as a working fluid around 3 €/m [54], employing the SiO_2 nanoparticle with 0.5% volumetric concentration increases more than 93% the cost of the GCHP system. It should be noted that this increment is only due to the capital cost of nanoparticle, not nanofluid, which will be also higher for the latter. Furthermore, a comparison between obtained

results for ΔL (Fig. 8) and C_{np} (Fig. 9) indicates that if the main objective of utilising nanofluids in GCHP systems is to reduce the required BHE length, their use is not economically viable.

4.2. Optimisation of ΔR_b

In the previous section, thermal performance of different nanofluids was compared by evaluating the *Mo* number, BHE effectiveness and the decrement percentage of the BHE thermal resistance, ΔR_b, under equivalent conditions. However, the latter (ΔR_b) is strongly dependent upon the thermal properties of the borehole and the ground, as well as on the physical arrangement of the BHE components. In this section, we examine integrated effects of different parameters on the reduction of the BHE thermal resistance for a nanofluid that showed promising thermal performance in previous section, namely Cu-water. A sensitivity analysis on the results obtained through the numerical simulations is performed in order to find conditions in which the optimum decrement of thermal resistance in presence of nanofluids can be achieved.

Figure 11 illustrates the evolution of the normalised BHE thermal resistance, defined as $R^*=R_{bf}/R_{nf}$, for different volume fractions of nanofluid over the logarithmic time scale. The figure shows a higher value of R^* for higher values of φ, namely a higher reduction of the thermal resistance, in both transient and quasi-stationary regimes. It is evident from the figure that, for all volume fractions, values of R^* reach an asymptotic value (steady-flux state) after 4 h of the operation. However, the obtained results show that this time for R_{nf} does not exceed 2 h (smaller denominator of R^*). The figure shows that employing nanofluids with the volume fraction lower than 0.5% are not promising for reduction of the BHE thermal resistance (ΔR_b less than 1%). In addition, elaboration of the results indicate that the decrement rate of thermal resistance does not alter linearly with the volume fraction; as φ increases the decrement rate of the thermal resistance decreases.

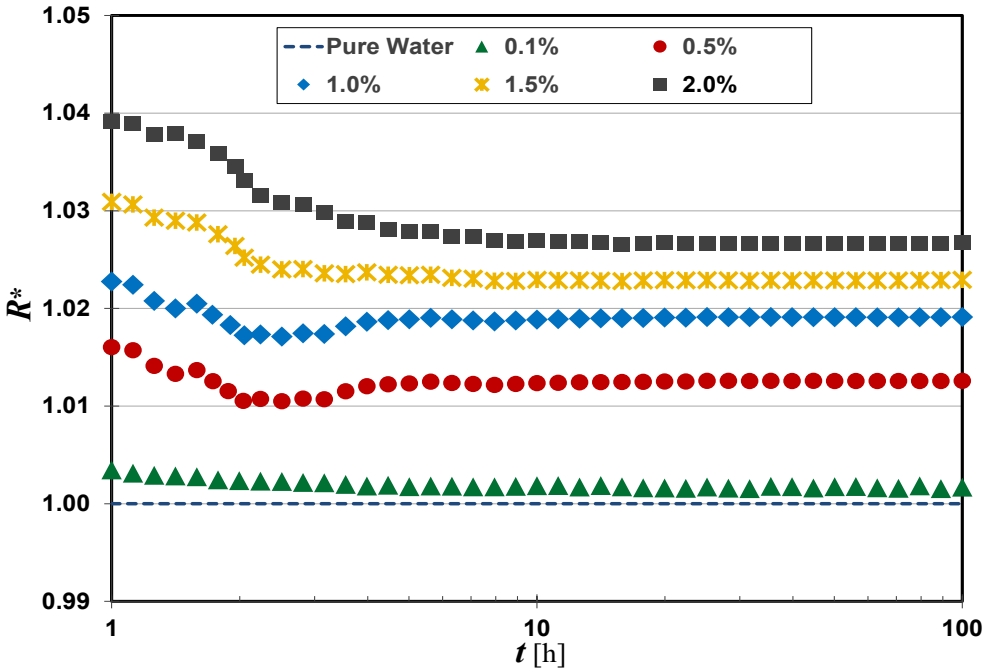

Fig. 11. Evolution of the normalised borehole thermal resistance, R^*, versus the logarithmic scale of time for different volume fractions of Cu-water nanofluid.

The integrated effects of the volume flow rate and dimensionless thermal conductivity, defined as $\sigma=(k_{gt}-k_{gd})/(k_{gt}+k_{gd})$, on the decrement percentage of thermal resistance (ΔR_b) for two volume fractions of nanofluid is illustrated in Fig. 12. The results for both nanofluid fractions indicate that a lower volume flow rate and a larger value of σ leads to a better reduction in the BHE thermal resistance (up to about 4%). The figure shows that a simultaneous increment of the thermal conductivity of ground and grout enhances the reduction of the BHE thermal resistance. However, the sensitivity analysis on the results revealed that the grout thermal conductivity is a more effective parameter than the ground thermal conductivity in any nanofluid fraction.

In terms of the volume flow rate, a higher reduction in the thermal resistance for lower flow rates can be justified by the exponential decrease of the convective film resistance with increase of the heat transfer coefficient ($R_c=1/\pi D_i\, h_{nf}$). In addition, a comparison between Fig. 12 (a) and (b) elucidates that, for a given value of σ, impact of increasing the nanofluid fraction on ΔR_b is more significant when the volume flow rate is lower. For instance, by increasing φ from 1% to 2%, ΔR_b at $\dot{V}$=10 *l*/min becomes 1.41 times larger, while this improvement at $\dot{V}$=30 *l*/min reduces to 1.27 times. These percentages remain almost equal in any value of σ.

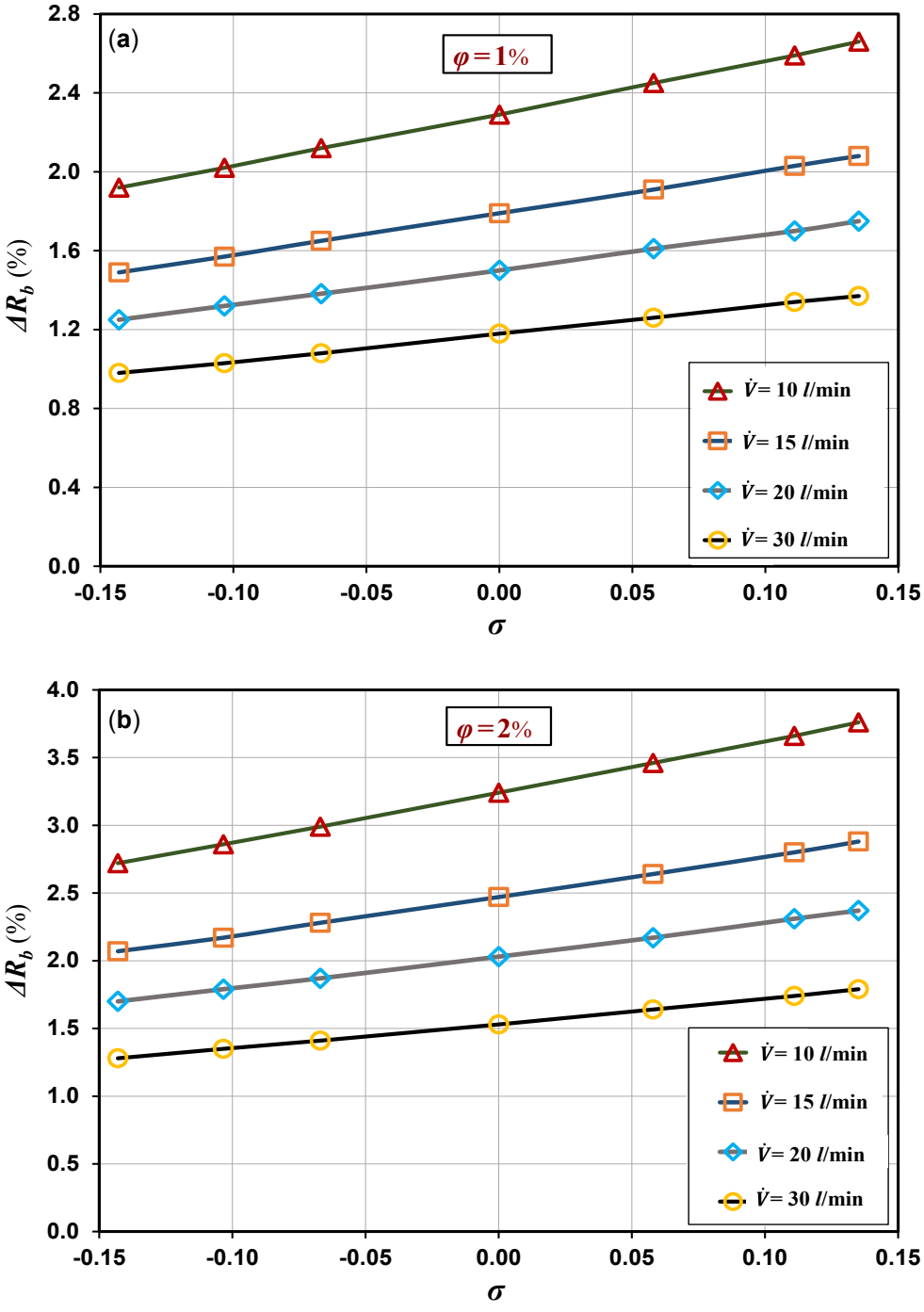

Fig. 12. Variation of the decrement percentage of thermal resistance (ΔR_b) with dimensionless thermal conductivity σ at different volume flow rates: φ=1% (a) and φ=2% (b).

Figure 13 shows the variations in ΔR_b triggered by alterations in values of the shank spacing (s) and nanofluid fraction at various volume flow rates. The figure shows that, for an intermediate values of s and $\dot{V}$, increasing φ from 0.5 % to 2.0% improves ΔR_b by 1.1%. On the other hand, for

an intermediate value of $\dot{V}$ and φ (1.0%), increasing s from 85 mm to 105 mm results in only 0.16% enhancement of ΔR_b. For any value of shank spacing, it is noticeable that the increase in nanofluid concentration increases the difference of ΔR_b between different volume flow rates. The figure indicates that the improvement of ΔR_b by increasing s can be considered meaningful only when $\dot{V}$ is minimum (10 l/min) and φ is larger than 1.0%. Therefore, in terms of shank spacing, the optimum improvement of ΔR_b occurs by higher values of s and φ in conjunction with lower values of $\dot{V}$.

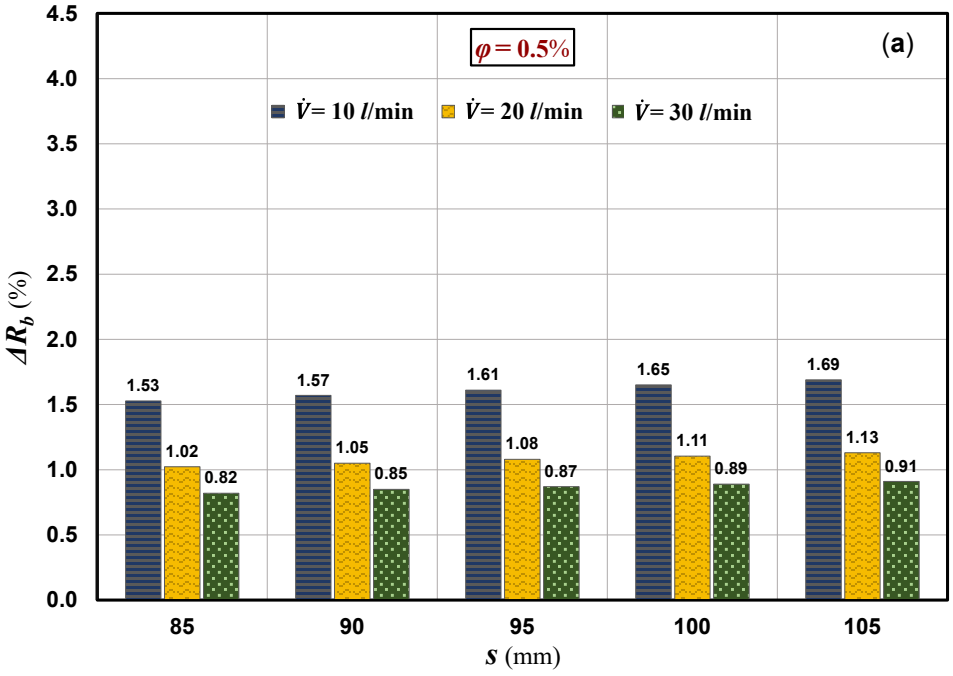

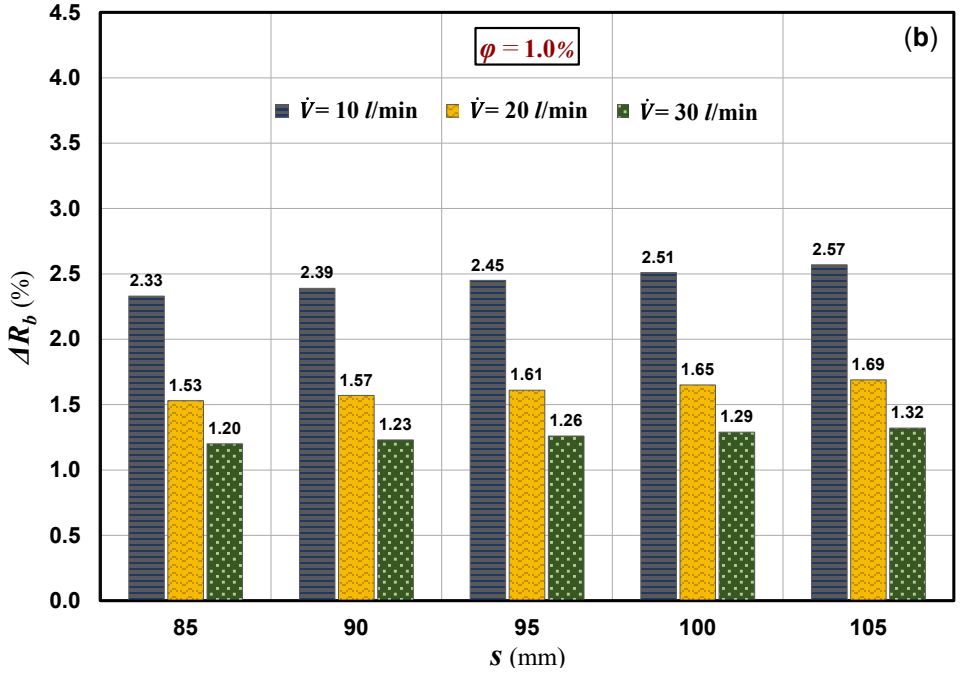
(b)
φ = 1.0%
V̇= 10 l/min
V̇= 20 l/min
V̇= 30 l/min
ΔR_b (%)
4.5
4.0
3.5
3.0
2.5
2.0
1.5
1.0
0.5
0.0
2.33
1.53
1.20
2.39
1.57
1.23
2.45
1.61
1.26
2.51
1.65
1.29
2.57
1.69
1.32
85
90
95
100
105
s (mm)

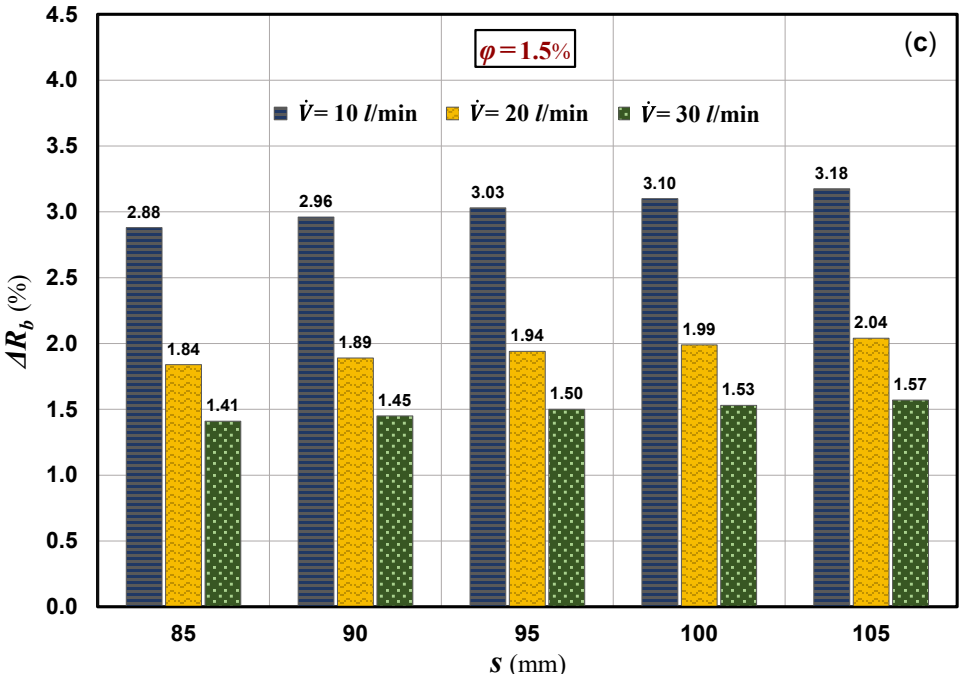
(c)
φ = 1.5%
V̇= 10 l/min
V̇= 20 l/min
V̇= 30 l/min
ΔR_b (%)
4.5
4.0
3.5
3.0
2.5
2.0
1.5
1.0
0.5
0.0
2.88
1.84
1.41
2.96
1.89
1.45
3.03
1.94
1.50
3.10
1.99
1.53
3.18
2.04
1.57
85
90
95
100
105
s (mm)

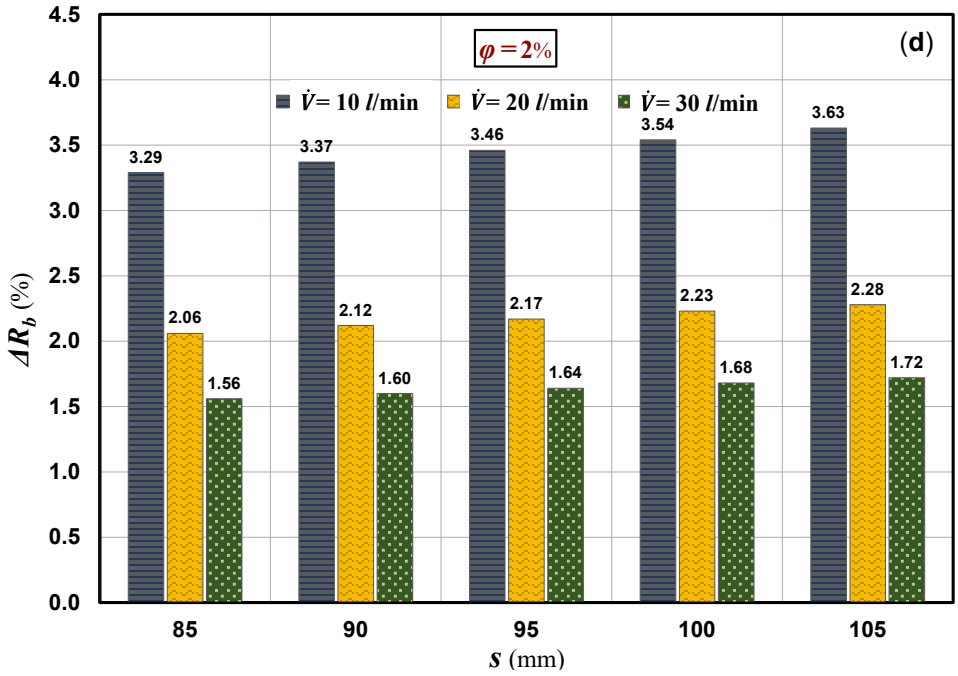

Fig. 13. Combined effects of the shank spacing (s) and the volume fraction of nanofluids on the decrement percentage of thermal resistance (ΔR_b) at different volume flow rates: φ=0.5% (a) - φ=2.0% (d).

Figure 14 compares the variation of ΔR_b with respect to different ratios of the borehole to pipe diameter, namely $\delta = D_b / D_i$, for three nanofluid fractions. The figure shows that decreasing the ratio δ results in a better decrement percentage of thermal resistance in any nanofluid fraction. Nonetheless, it can be observed that the diagram of a larger φ decreases with a steeper slope, implying that role of the ratio δ in improvement of ΔR_b becomes more remarkable as the volume fraction increases. For example, the difference between the lowest and the highest ΔR_b at φ=2.0 % is 2.5 times greater than that at φ=0.5%.

From the results of Figs. 11-14, it can be asserted that the optimum decrement percentage of thermal resistance in presence of nanoparticles occurs by a lower volume flow rate and diameter ratio (borehole to pipe) in conjunction with a higher volume fraction of nanofluids, shank spacing and grout thermal conductivity. It is noteworthy to mention that for the considered operating conditions in this study (Table 1), the highest achieved decrement percentage of thermal resistance for the Cu-based nanofluid is 4.31%.

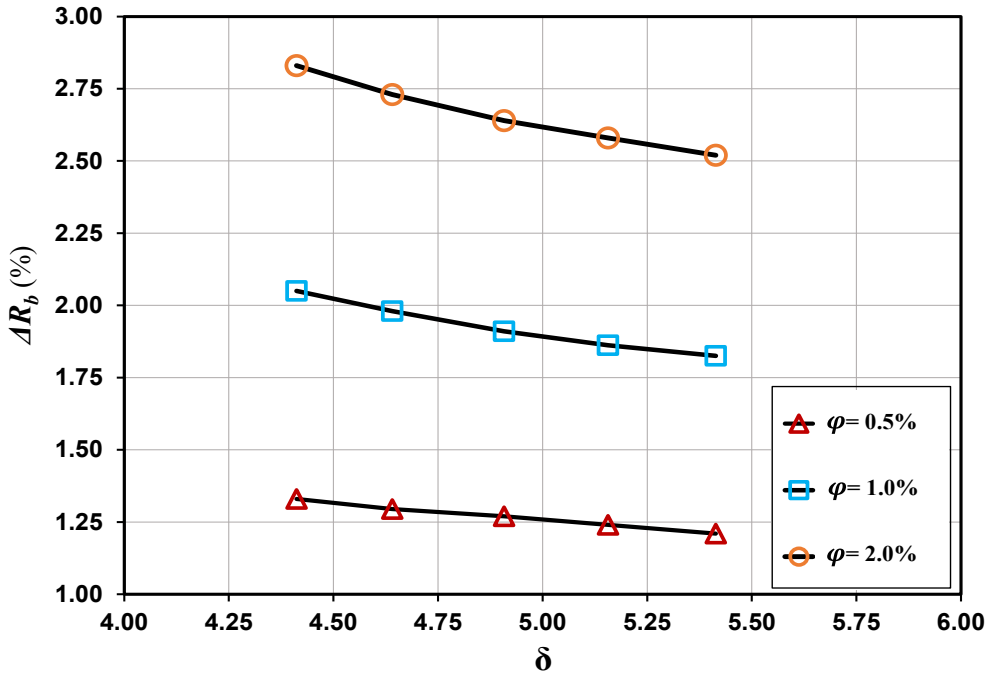

Fig. 14. Variation of the decrement percentage of thermal resistance (ΔR_b) with dimensionless diameter (δ) for φ=0.5, 1.0 and 2.0 %.

4.3. Outlet temperature of nanofluids

This section highlights the role of nanoparticles in variation of the outlet fluid temperature, T_{out}, of the BHE. Effects of the borehole length along with nanofluid concentration on the BHE effectiveness (ε) and decrement percentage of the outlet temperature ($\Delta\theta$) are addressed. Finally, simple equations are provided for evaluation of T_{out} for nanofluids.

Figure 15 illustrates the time evolution of T_{out} for different volumetric concentrations of Cu-water nanofluid as well the pure water for two borehole lengths, namely L=100 m and L=200 m. In order to enhance the readability of the chart, the results in the very first minutes of the operation are disregarded and the results are magnified for a time span between 40 and 50 h. A comparison between Figs. 15 (a) and 15 (b) shows the prominent impact of the BHE length in reduction of T_{out} (cooling condition): Almost 2.25 ºC lower values of T_{out} in the steady-flux state for the case with L=200 m, compared to values of T_{out} obtained for the case with L=100 m. However, in comparison with the BHE length, the figure shows that increasing the nanofluid concentration has a slight effect on the reduction of outlet temperature of nanofluids with respect to the pure water. For both lengths, the maximum temperature reduction in steady-flux state, with respect to pure water, does

not exceed 0.05ºC. It should be added this trend was also observed for other nanofluids with a scant discrepancy with respect to the present case.

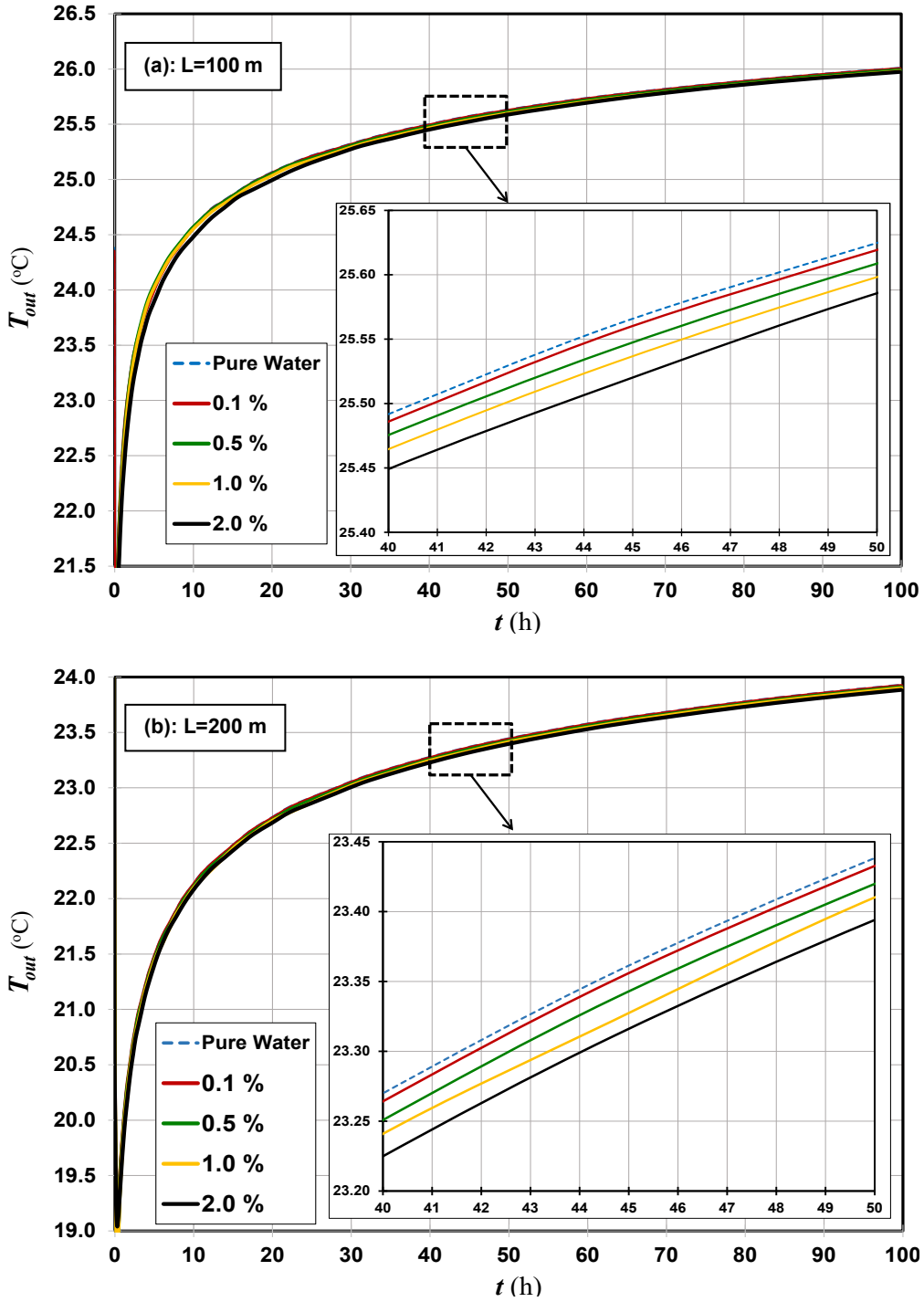

Fig. 15. Time evolution of the outlet fluid temperature T_{out} for different volumetric concentrations of the Cu-water nanofluid and pure water: L=100 m (a) and L=200 m (b).

Figure 16 compares the BHE effectiveness coefficients (ε) as a function of T_{out} and corresponding values of the decrement percentage of the outlet temperature ($\Delta\theta$) for different borehole lengths and volumetric concentrations of Cu-water nanofluid. The figure shows that the BHE effectiveness improves in any BHE length with the volumetric concentration of nanofluid, and that the value of ε is considerably dependent upon the borehole length. The results show that increasing the BHE length from 50 to 100 m leads to a 79% improvement of the BHE effectiveness. Nevertheless, the enhancement rate of the effectiveness due to the increase in BHE length is independent of the volumetric concentration. Furthermore, it can be observed that $\Delta\theta$ is an increasing function of the volume fraction of nanofluid for any length. However, the role of nanofluid concentration in enhancement of $\Delta\theta$ becomes more striking as borehole length increases.

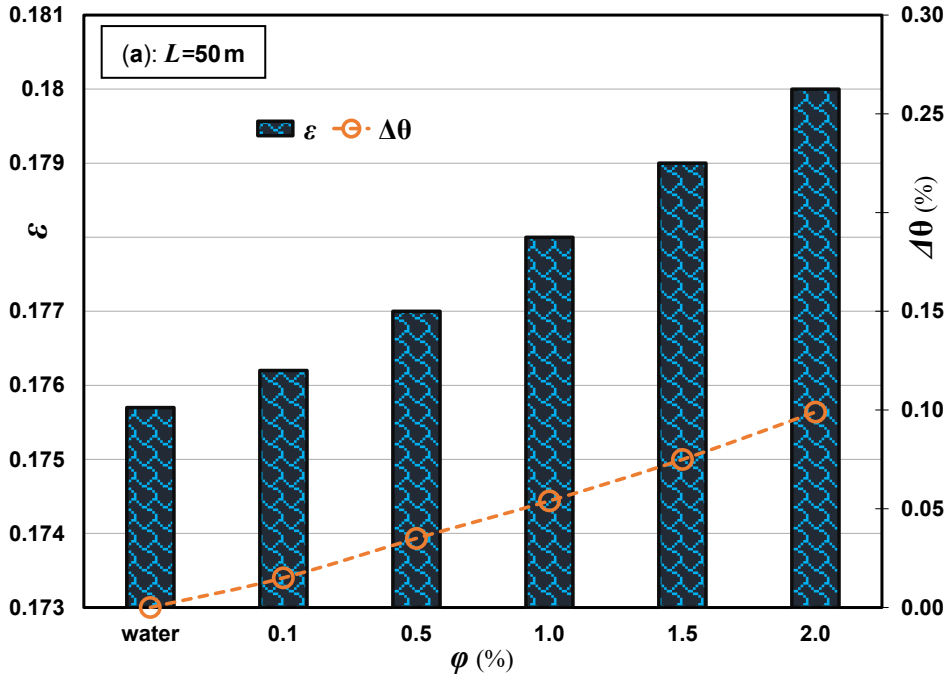

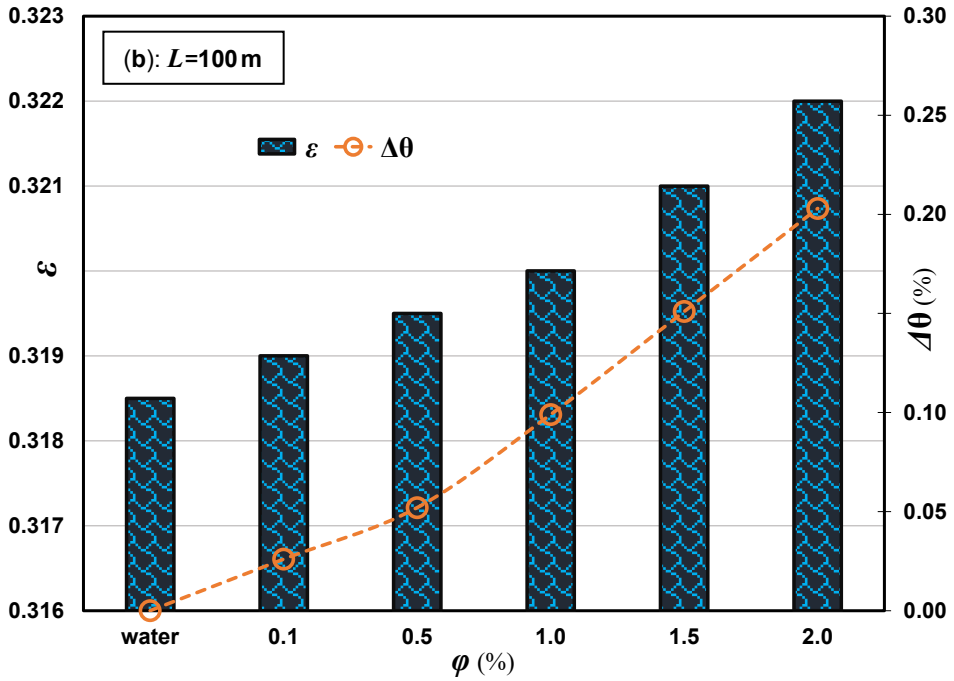
(b): L=100 m
ε
Δθ
0.323
0.322
0.321
0.319
0.318
0.317
0.316
0.30
0.25
0.20
0.10
0.05
0.00
Δθ (%)
water
0.1
0.5
1.0
1.5
2.0
φ (%)

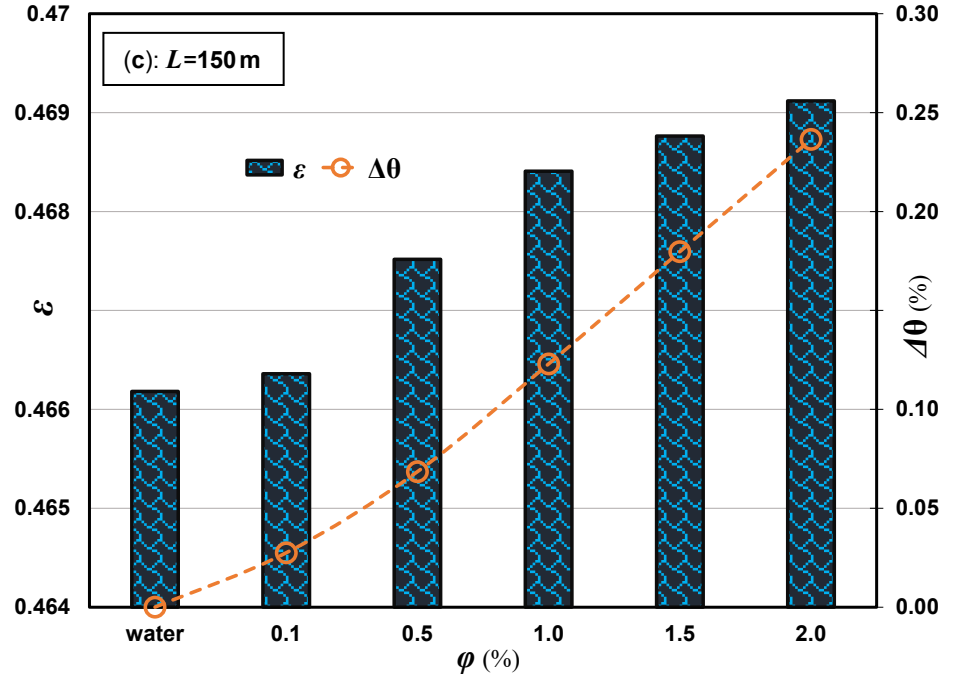
(c): L=150 m
ε
Δθ
0.47
0.469
0.468
0.466
0.465
0.464
0.30
0.25
0.20
0.10
0.05
0.00
Δθ (%)
water
0.1
0.5
1.0
1.5
2.0
φ (%)

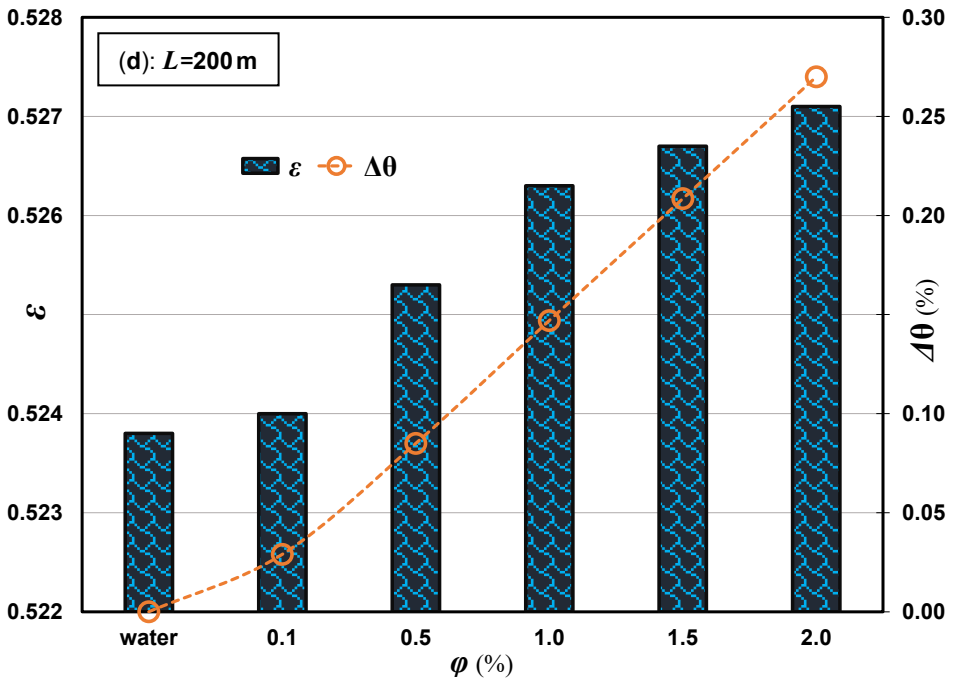

Fig. 16. Comparison of the effectiveness and decrement percentage of the outlet temperature for different concentrations of Cu-water nanofluid: Effect of the BHE length, L=50 m (a) – 200 m (d).

Indeed, the outlet fluid temperature, T_{out}, is a key parameter reflecting the borehole performance and its time evolution is essential for the dynamic simulation of GCHP systems. Thus, it would be interesting to have correlations without the need of complicated calculation algorithms in order to evaluate T_{out} for BHEs employing nanofluids as a working fluid. In the present study, by means of the best-fitting interpolation of 3D simulation results, obtained for various nanofluids under different conditions, we propose simple equations to calculate the outlet fluid temperature of nanofluids.

Most of the short-term or full-time-scale simulation models in the literature yield directly the time evolution of mean fluid temperature, T_m, for a borefield subjected to a time constant heat load. Nonetheless, they do not yield directly the time evolution of the fluid temperature at the outlet of the BHEs, T_{out}. In previous studies [55, 56], it was shown that for a given volume flow rate, the difference of inlet and outlet fluid temperature (T_{in}–T_{out}) is proportional to the difference of arithmetic average and mean fluid temperature (T_{ave}–T_m), where T_m is determined by Eq. (17) and T_{ave}=(T_{in}+T_{out})/2. It was found that the ratio (T_{ave}–T_m)/(T_{in}–T_{out}) is time independent in the steady-flux regime. The validity of this ratio was shown for different values of the ground and grout thermal conductivity, BHE diameter and length, and shank spacing, in any operating condition

including winter-heating and summer-cooling as well as TRTs (thermal response tests). This ratio can be introduced by the dimensionless coefficient ψ:

$$\psi = \frac{T_{ave} - T_m}{T_{in} - T_{out}} \tag{30}$$

By means of the linear regression of 3D simulation results, we obtained a dimensionless expression to calculate the coefficient ψ for nanofluids, which is given as:

$$\psi = \frac{1}{5\dot{V}^*}\left[0.129L^* + 0.0233\frac{k^*}{s^*} + 0.0774\frac{L^*k^*}{s^*} + 0.0128\right] \tag{31}$$

where $\dot{V}^*$, L^*, k^* and s^* are dimensionless parameters defined as:

$$\dot{V}^* = \dot{V} / \dot{V}_0 \;;\; L^* = L / L_0 \;;\; k_{gt}{}^* = k_{gt} / k_{gt} \;;\; s^* = s / s_0. \tag{32}$$

In Eq. (32), L_0, k_{gt0} and d_0 are reference values of the BHE length, grout thermal conductivity, and shank spacing, and are equal to: $\dot{V}$=10 *l*/min, L_0 = 50 m, k_{gt0} = 1.2 W/(mK), and d_0 = 85 mm.

In quasi-stationary working conditions, the energy balance equation for a BHE employing nanofluids can be expressed as below:

$$T_{in} - T_{out} = \frac{\dot{Q}}{\dot{m}_{nf} c_{p,nf}} \tag{33}$$

where $\dot{Q}$ is the thermal power exchanged between the heat pump and the borehole fluid, $\dot{m}_{nf}$ is the mass flow rate of nanofluid, and $c_{p,nf}$ is the specific heat capacity at constant pressure of nanofluid. By substituting Eq. (30) in the energy balance equation, one yields:

$$T_{out} = \left(\psi - \frac{1}{2}\right)\frac{\dot{Q}}{\dot{m}_{nf} c_{p,nf}} + T_m \tag{34}$$

By inserting the definition of *Pe* number in Eq. (34), defined as $Pe_{nf} = Re_{nf}.Pr_{nf}$, it can be rewritten in the following form:

$$T_{out} = \frac{(4\psi - 2)\dot{Q}}{\pi D_i k_{nf} Pe_{nf}} + T_m \tag{35}$$

where in Eq. (35) the thermal conductivity of nanofluids, k_{nf}, can be estimated through Eq. (10). In Eq. (35), the time evolution of mean fluid temperature, T_m, can be calculated either by applying the available analytical correlations [57-59] or by simulation codes. Equations (31) and (35) allow

a simple calculation of the outlet fluid temperature in quasi-stationary working conditions, for single U-tube BHEs employing nanofluids as heat carrier fluids.

Table 6. Details of cases considered to demonstrate the validity of Eq. (35).

Case no.	Nanofluid	φ (%)	L (m)	D_b (cm)	s (mm)	$\dot{V}$ (l/min)	k_{gd} (W/(m.K))	k_{gt} (W/(m.K))
1	Al_2O_3	1.5	110	16.0	95	12	2.0	1.5
2	Ag	0.5	50	15.0	90	14	1.8	1.8
3	SiO_2	2.0	80	15.5	85	18	2.2	1.6
4	CuO	1.0	140	16.5	100	10	2.4	1.4

In order to show the validity of Eq. (35) for various types of nanofluids under different operating conditions, the time evolution of T_{out} are compared between four different cases. Details of the considered cases are reported in Table 6. Figure 17 illustrates the evolution of T_{out} in the logarithmic scale of time for different cases (Table 6), yielded by 3D simulations (denoted by Sim) and those obtained by applying Eq. (35) (denoted by Eq.). A comparison between graphs confirms the accuracy of proposed equations in calculation of T_{out} for different nanofluid cases. The highest root-mean-square-deviation (RMSD) of results obtained through Eq. (35) from those yielded by 3D simulations is 0.089 ºC corresponding to Case 4.

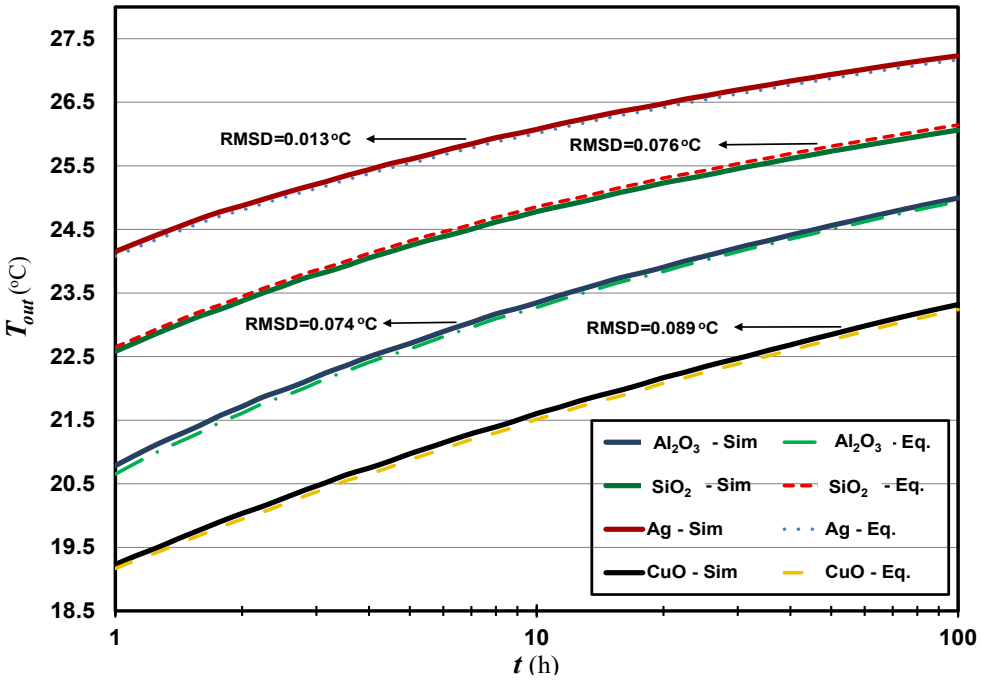

Fig. 17. Comparison of the time evolution of outlet temperature T_{out} between cases reported in Table 6: 3D simulation vs. Eq. (35).

To validate the results obtained through Eq. (35) with the available literature data, the numerical results of Javadi et al. [30] were selected to be compared with those yielded by Eq. (35). Their results were obtained for a hybrid nanofluid, namely Ag-MgO/water, at Re=3200 and T_{in}=27°C, and with 0.5% volumetric concentration. Considered values of the thermophysical properties, the operating condition, and the BHE characteristics can be found in Ref. [30]. Figure 18 demonstrates the evolution of T_{out} over 24 h operation yielded through 3D numerical simulations, by applying Eq. (35) as well as those presented by Javadi et al. [30]. For calculation of T_{out} through Eq. (35), values of the mean fluid temperature (T_m) were obtained by applying the analytical model proposed by Man et al. [58], which is not given here for the sake of brevity. The results of Fig. 18 shows a good agreement between values of T_{out} yielded through Eq. (35) and those either given in Ref. [30] or obtained by the 3D simulation. The root-mean-square-deviations of the results obtained through Eq. (35) and 3D simulations from those given in [30] are 0.027 °C and 0.016 °C, respectively.

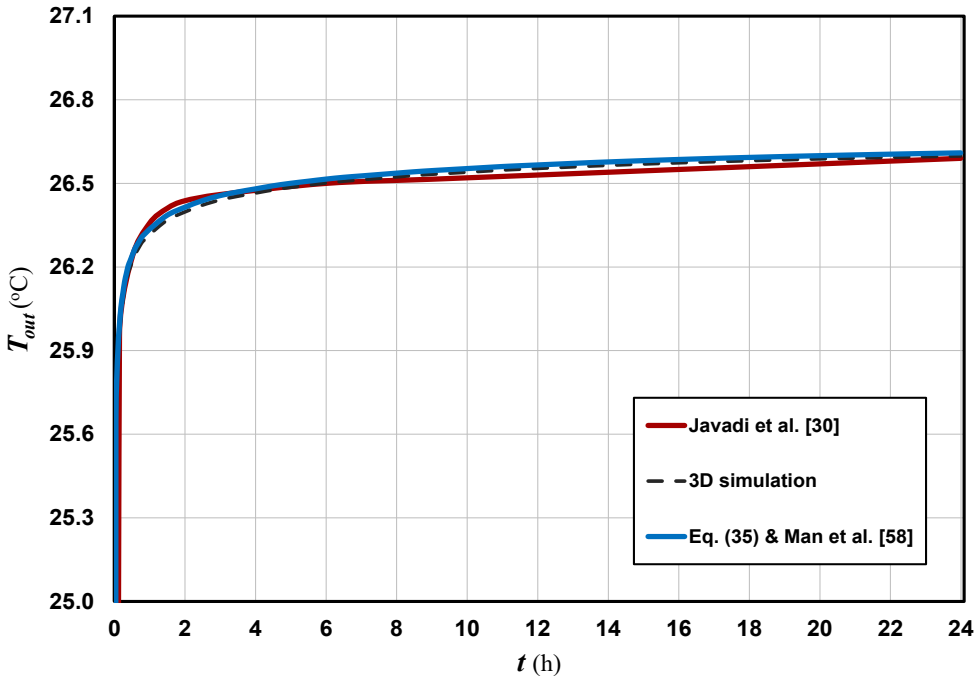

Fig. 18. Comparison between time evolutions of the outlet temperature, T_{out}, obtained through Eq. (35), 3D simulation and those given in [30].

5. Conclusions

The present study dealt with a comprehensive performance evaluation of single U-tube borehole heat exchangers (BHEs) using nanofluids as the circuit fluid. Several performance indicators were introduced and the BHE performance in presence of seven common nanofluids were compared by means of 3D finite element simulations. Firstly, a comparative techno-economic analysis was performed to highlight the merits or drawbacks of each nanofluid. Then, a sensitivity analysis was performed to find conditions in which an optimum decrement percentage of the BHE thermal

resistance is achieved. Finally, elaboration of the results through the best fitting technique allowed to propose simple equations for calculation of the outlet fluid temperature in single U-tube BHEs utilising nanofluids. The main findings of the present study can be concluded as follows:

1- It was revealed that for volume fractions lower than 0.5%, the difference between heat transfer enhancements of different nanofluids is marginal. The Ag- and Cu-water nanofluids were characterised by the best thermal performance among all nanofluids, including the highest *Mo* number (convective heat transfer), COP improvement factor, and decrement percentage of thermal resistance in any volume fraction. However, this better thermal performance was at the penalty of higher pressure drop and, consequently, up to about 31% higher required pumping power, with respect to the water. On the other hand, SiO_2-based nanofluid followed by TiO_2-water nanofluid were the worst cases in terms of the thermal performance, but at the same time, they were characterised by the lowest pressure drop.

2- The results indicated that employing the nanofluids is not promising for the purpose of reducing the borehole length. The Ag- and SiO_2-based nanofluids showed the highest reduction in borehole length which was only about 1.5% at volume fraction of 2%. It was also shown that the possible decrement percentage of BHE length is proportional to enhancement of the BHE effectiveness.

3- Economic analysis revealed that the cost of electrical energy for nanofluids due to a higher energy consumption of pump is negligible, compared to the capital cost of nanoparticles. Comparisons between results implied that if the main objective of utilising nanofluids in GCHP systems is to reduce the required BHE length, their use is not economically viable.

4- The SiO_2 nanoparticle with a capital cost ranging from 5.8 to 17.5 €/m was the cheapest nanoparticle, while Ag and Cu nanoparticles were the most expensive ones. In addition, the costs of Fe_2O_3 and TiO_2 nanoparticles were close to the cheapest nanoparticle, namely SiO_2. Although employing the Ag-based nanofluid in BHEs is advantageous in terms of the thermal performance, its extremely high capital cost is a major hindrance for its utilisation in GCHP systems.

5- It can be concluded that the optimum decrement percentage of thermal resistance in presence of nanoparticles occurs by a lower volume flow rate and diameter ratio (borehole to pipe) in conjunction with a higher volume fraction of nanofluids, shank spacing and grout thermal conductivity. The highest decrement percentage of thermal resistance for the Cu-based nanofluid was equal to 4.31%.

6- The proposed equations showed an appropriate accuracy in evaluation of the outlet fluid temperature for any nanofluid under different working conditions. Moreover, the obtained results indicated that the role of nanofluid concentration in enhancement of the outlet temperature becomes more striking as the BHE length increases.

Findings of the present study are expected to provide an insight into potential application of nanofluids in GCHP systems. A recommendation for future works is to analyse the long-term performance of nanofluids in both single and double U-tube BHEs coupled to a GCHP system, in order to understand their applicability and potentiality in the whole system.

References

[1] J. Lund and T. Boyd, "Direct Utilization of Geothermal Energy 2015 worldwide review," *Geothermics,* vol. 60, pp. 66-93, 2016.

[2] L. Aresti, P. Christodoulides and G.Florides, "A review of the design aspects of ground heat exchangers," *Renewable and Sustainable Energy Reviews,* vol. 92, pp. 757-773, 2018.

[3] E. Atam and L. Helsen, "Ground-coupled heat pumps: Part 2 - Literature review and research challenges in optimal design," *Renewable and Sustainable Energy Review,* vol. 54, pp. 1668-1684, 2015.

[4] E. Dube Kerme and A. Fung, "Transient heat transfer simulation, analysis and thermal performance study of double U-tube borehole heat exchanger based on numerical heat transfer model," *Applied Thermal Engineering,* vol. 173, p. 115189, 2020.

[5] B. Bouhacina, R. Saim , H. Benzenine and H.F. Oztop, "Analysis of thermal and dynamic comportment of a geothermal vertical U-tube heat exchanger," *Energy and Buildings,* Vol. 58, p. 37-43, 2013.

[6] F. Ruiz-Calvo, C. Montagud, A. Cazorla-Marín and J. Corberán, "Development and Experimental Validation of a TRNSYS Dynamic Tool for Design and Energy Optimization of Ground Source Heat Pump Systems," *Energies,* vol. 10, no. 10, p. 1510, 2017.

[7] M. Rivoire, A. Casasso, B. Piga and R. Sethi, "Assessment of Energetic, Economic and Environmental Performance of Ground-Coupled Heat Pumps," *Energies,* vol. 11, p. 1941, 2018.

[8] C. Naranjo-Mendoza, M. Oyinlolab, A. Wright and R. Greenough, "Experimental study of a domestic solar-assisted ground source heat pump with seasonal underground thermal energy storage through shallow boreholes," *Applied Thermal Engineering,* vol. 162, p. 114218, 2019.

[9] M. Samson, J. Dallaire and L. Gosselin, "Influence of groundwater flow on cost minimization of ground coupled heat pump systems," *Geothermics,* vol. 73, pp. 100-110, 2018.

[10] P. Blum, G. Campillo and T. Kölbel, "Techno-economic and spatial analysis of vertical ground source heat pump systems in Germany," *Energy,* vol. 36, pp. 3002-3011, 2011.

[11] F. Robert and L. Gosselin, "New methodology to design ground coupled heat pump systems based on total cost minimization," *Applied Thermal Engineering,* vol. 62, no. 2, pp. 481-491, 2014.

[12] S. Javed and J. Spitler, "Accuracy of borehole thermal resistance calculation methods for grouted single U-tube ground heat exchangers," *Applied Energy,* vol. 187, pp. 790-806, 2017.

[13] F. Chen, J. Mao, S. Chen, C. Li, P. Hou and L. Liao, "Efficiency analysis of utilizing phase change materials as grout for a vertical U-tube heat exchanger coupled ground source heat pump system," *Applied Thermal Engineering,* vol. 130, pp. 698-709, 2018.

[14] R. Bassiouny, M. Ali and M. Hassan, "An idea to enhance the thermal performance of HDPE pipes used for ground-source applications," *Applied Thermal Engineering,* vol. 109, pp. 15-21, 2016.

[15] G. Emmi, A. Zarrella, M. De Carli, M. Donà and A. Galgaro, "Energy performance and cost analysis of some borehole heat exchanger configurations with different heat-carrier fluids in mild climates," *Geothermics,* vol. 65, pp. 158-169, 2017.

[16] A. Serageldin, Y. Sakata, T. Katsura and N. Katsunori, "Performance enhancement of borehole ground source heat pump using single U-tube heat exchanger with a novel oval cross-section (SUO) and a novel spacer," *Sustainable Energy Technologies and Assessments,* vol. 42, p. 100805, 2020.

[17] M. Goodarzi, A. S. Kherbeet, M. Afrand and et al., "Investigation of heat transfer performance and friction factor of a counter-flow double-pipe heat exchanger using nitrogen-doped, graphene-based nanofluids," *International Communications in Heat and Mass Transfer,* vol. 76, pp. 16-23, 2016.

[18] M. M. Sarafraz, M. R. Safaei, Z. Tian and et al., "Thermal Assessment of Nano-Particulate Graphene-Water/Ethylene Glycol (WEG 60:40) Nano-Suspension in a Compact Heat Exchanger," *Energies,* vol. 12, no. 10, p. 1929, 2019.

[19] Z. X. Li, U. Khaled, A.A.A. Al-Rashed and et al., "Heat transfer evaluation of a micro heat exchanger cooling with spherical carbon-acetone nanofluid," *International Journal of Heat and Mass Transfer,* vol. 149, p. 119124, 2020.

[20] M. Goodarzi, A. Amiri, M. S. Goodarzi and et al., "Investigation of heat transfer and pressure drop of a counter flow corrugated plate heat exchanger using MWCNT based nanofluids," *International Communications in Heat and Mass Transfer,* vol. 66, pp. 172-179, 2015.

[21] D. Sui, V. Langåker and Z. Yu, "Investigation of thermophysical properties of nanofluids for application in geothermal energy," *Energy Procedia,* vol. 105, pp. 5055-5060, 2017.

[22] M. Daneshipour and R. Rafee, "Nanofluids as the circuit fluids of the geothermal borehole heat exchangers," *International Communications in Heat and Mass Transfer,* vol. 81, pp. 34-41, 2017.

[23] X.-H. Sun, H. Yan, M. Massoudi, Z.-H. Chen and W.-T. Wu, "Numerical simulation of nanofluid suspensions in a geothermal heat exchanger," *Energies,* vol. 11, no. 4, p. 919, 2018.

[24] R. Du, D. Jiang and Y. Wang, "Numerical investigation of the effect of nanoparticle diameter and sphericity on the thermal performance of geothermal heat exchanger using nanofluid as heat transfer fluid," *Energies,* vol. 13, p. 1653, 2020.

[25] R. Du, D. Jiang, Y. Wang and K. Shah, “An experimental investigation of CuO/water nanofluid heat transfre in geothermal heat exchanger,” *Energy and Buildings,* vol. 227, p. 110402, 2020.

[26] A. Kapıcıoğlu and H. Esen, “Experimental investigation on using Al2O3/ethylene glycol-water nano-fluid in different types of horizontal ground heat exchangers,” *Applied Thermal Engineering,* vol. 165, p. 114559, 2020.

[27] H. Narei, R. Ghasempour and Y. Noorollahi, “The effect of employing nanofluid on reducing the bore length of a vertical ground-source heat pump,” *Energy Conversion and Management,* vol. 123, pp. 581-591, 2016.

[28] G. Digilio, C. Roselli, M. Sasso and U. Channabasappa, “Borehole heat exchanger with nanofluids as heat carrier,” *Geothermics,* vol. 72, pp. 112-123, 2018.

[29] A. Jahanbin, G. Semprini and B. Pulvirenti, “Nanofluid suspensions as heat carrier fluids in single U-tube borehole heat exchangers,” *Journal of Physics: Conference Series ,* vol. 2116, p. 012100, 2021.

[30] H. Javadi, J. Urchueguia, S. Ajarostaghi and B. Badenes , “Impact of employing hybrid nanofluids as heat carrier fluid on the thermal performance of a borehole heat exchanger,” *Energies,* vol. 14, p. 2892, 2021.

[31] A. Jahanbin, “Thermal performance of the vertical ground heat exchanger with a novel elliptical single U-tube,” *Geothermics,* vol. 86, p. 101804, 2020.

[32] NIST, “Thermophysical properties of fluid systems, http://webbook.nist.gov/chemistry/fluid”.

[33] A. Jahanbin, G. Semprini, A.N. Impiombato, C. Biserni and E.R. di Schio, “Effects of the circuit arrangement on the thermal performance of double U-tube ground heat exchangers,” *Energies,* vol. 13, no. 12, p. 3275, 2020.

[34] Y. Xuan and W. Roetzel, “ Conceptions for heat transfer correlation of nanofluids,” *International Journal of Heat and Mass Transfer,* vol. 43, no. 19, pp. 3701-3707, 2000.

[35] M. R. Safaei, A. Jahanbin, A. Kiani and et al., “Mathematical modeling for nanofluids simulation: a review of the latest works,” in *Modeling and Simulation in Engineering Sciences*, InTechOpen, 2016.

[36] W. Yu and S. Choi, “ The role of interfacial layers in the enhanced thermalconductivity of nanofluids: a renovated Maxwell model,” *Journal of Nanoparticle Research,* vol. 5, pp. 167-171, 2003.

[37] B. Pak and Y. Cho, “Hydrodynamic and heat transfer study of dispersed fluids with submicron metalic oxide particles,” *Experimental Heat Transfer,* vol. 11, pp. 151-170, 1998.

[38] X. Wang, X. Xu and S. Choi, “Thermal conductivity of nanoparticles-fluid mixture,” *Journal of Thermophysics and Heat Transfer,* vol. 13, no. 4, 1999.

[39] J. Olson, “Nanofluids and a method of making nanofluids for ground source heat pumps and other applications”, 2013.

[40] E. Zanchini and A. Jahanbin, "Effects of the temperature distribution on the thermal resistance of double u-tube borehole heat exchangers," *Geothermics,* vol. 71, pp. 46-54, 2018.

[41] P. Hu, Z. Yu, N. Zhu, F. Lei and X. Yuan, "Performance study of a ground heat exchanger based on the multipole theory heat transfer model," *Energy and Buildings,* vol. 65, pp. 231-241, 2013.

[42] J. Jalaluddin and A. Miyara, "Thermal performance and pressure drop of spiral-tube ground heat exchangers for ground-source heat pump," *Applied Thermal Engineering,* vol. 90, p. 630–637, 2015.

[43] R. Vajiha, D. Das and D. Kulkarni, "Development of new correlations for convective heat transfer and friction factor in turbulent regime for nanofluids," *International Journal of Heat and Mass Transfer,* vol. 53, no. 15-16, pp. 4607-4618, 2010.

[44] Y. Peng, Y. Wang and R. Du, "The effects of nanofluid to vertical single U-tube ground heat exchanger," in *Proceeding of BSO, 4th Building Simulation and Optimization Conference*, Cambridge, UK, 2018.

[45] S. Shamshirgaran, H. Al-Kayiem, K. Sharma and M. Ghasemi, "State of the art of techno-economics of nanofluid-laden flat-plate solar collectors for sustainable accomplishment," *Sustainability,* vol. 12, p. 9119, 2020.

[46] S. Wciślik, "A simple economic and heat transfer analysis of the nanoparticles use," *Chemical Papers,* vol. 71, pp. 2395-2401, 2017.

[47] "Nanostructured & Amorphous Materials, Inc.," [Online]. https://www.nanoamor.com/elements__oxides__carbides___nitrides_nanoparticles.

[48] "Eorostat - Statistics Explained," [Online]. https://ec.europa.eu/eurostat/statisticsexplained/index.php?title=Electricity_price_statistics.

[49] J. Jalaluddin, A. Miyara, K. Tsubaki, S. Inoue and K. Yoshida, "Experimental study of several types of ground heat exchanger using a steel pile fundation," *Renewable Energy,* vol. 36, pp. 764-771, 2011.

[50] W. Duangthongsuk and S. Wongwises, "An experimental study on the heat transfer performance and pressure drop of TiO2-water nanofluids flowing under a turbulent flow regime," *International Journal of Heat and Mass Transfer,* vol. 53, pp. 334-344, 2010.

[51] S. Javed, H. Ali, H. Babar, M. Khan, M. Janjua and M. Bashir, "Internal convective heat transfer of nanofluids in different flow regimes: A comprehensive review," *Physica A: Statistical Mechanics and its Applications,* vol. 538, p. 122783, 2020.

[52] R. Vajjha, D. Das and D. Ray, "Development of new correlations for the Nusselt number and the friction factor under turbulent flow of nanofluids in flat tubes," *International Journal of Heat and Mass Transfer,* vol. 80, pp. 353-367, 2015.

[53] M. Kong, J. Alvarado, C. Thies, S. Morefield and C. Marsh, "Field evaluation of microencapsulated phase change material slurry in ground source heat pump systems," *Energy,* vol. 122, pp. 691-700, 2017.

[54] H. Esen, M. Inalli and M. Esen, “A techno-economic comparison of ground-coupled and air-coupled heat pump system for space cooling.,” *Building and Environment,* vol. 42, pp. 1955-1965, 2007.

[55] E. Zanchini and A. Jahanbin, “Correlations to determine the mean fluid temperature of double U-tube borehole heat exchangers with a typical geometry,” *Applied Energy,* vol. 206, pp. 1406-1415, 2017.

[56] E. Zanchini and A. Jahanbin, “Simple equations to evaluate the mean fluid temperature of double U-tube borehole heat exchangers,” *Applied Energy,* vol. 231, pp. 1406-1415, 2018.

[57] H. Zeng, N. Diao and Z. Fang, “Heat transfer analysis of boreholes in vertical ground heat exchangers,” *International Journal of Heat and Mass Transfer,* vol. 46, pp. 4467-4481, 2003.

[58] Y. Man, H. Yang, N. Diao, J. Liu and Z. Fang, “A new model and analytical solutions for borehole and pile ground heat exchangers,” *International Journal of Heat and Mass Transfer ,* vol. 53, p. 2593–2601, 2010.

[59] R. Beier and J. Spitler, “Weighted average of inlet and outlet temperatures in borehole heat exchangers,” *Applied Energy,* vol. 174, p. 118–129, 2016.